Air temperature equation derived from sonic temperature and water vapor mixing ratio for turbulent air flow sampled through closed-path eddy-covariance flux systems

Xinhua Zhou[1,2,3,4], Tian Gao[1,3,5*], Eugene S. Takle[3,7], Xiaojie Zhen[3,6], Andrew E. Suyker[4], Tala Awada[4], Jane Okalebo[4], Jiaojun Zhu[1,3,5]

[1]CAS Key Laboratory of Forest Ecology and Management, Institute of Applied Ecology, Chinese Academy of Sciences, Shenyang, 110016, China
[2]Campbell Scientific Inc., Logan, Utah 84321, USA
[3]CAS-CSI Joint Laboratory of Research and Development for Monitoring Forest Fluxes of Trace Gases and Isotope Elements, Institute of Applied Ecology, Chinese Academy of Sciences, Shenyang 110016, China
[4]University of Nebraska, Lincoln, Nebraska 68583, USA
[5]Qingyuan Forest CERN, ~~CAS~~ Chinese Academy of Sciences, Shenyang 110016, China
[6]Beijing Techno Solutions Ltd., Beijing 100088, China
[7]Iowa State University, Ames, Iowa 50011, USA

Correspondence to: Tian Gao (tiangao@iae.ac.cn)

Abstract. Air temperature (T) plays a fundamental role in many aspects of the flux exchanges between the atmosphere and ecosystems. Additionally, ~~it is critical to~~ knowing where (in relation to other essential measurements) and at what frequency T must be measured ~~to~~is critical to accurately describinge such exchanges. In closed-path eddy-covariance (CPEC) flux systems, T can be computed from the sonic temperature (T_s) and water vapor mixing ratio that are measured by the fast-response sensosrs of a three-dimensional sonic anemometer and infrared gas analyzer, respectively. T ~~then~~ is then computed by use of either $T = T_s(1+0.51q)^{-1}$, where q is specific humidity, or $T = T_s(1+0.32e/P)^{-1}$, where e is water vapor pressure and P is atmospheric pressure. Converting q and e/P into the same water vapor mixing ratio analytically reveals the difference between these two equations. This difference in a CPEC system could reach ±0.18 K, bringing an uncertainty into the accuracy of T from both equations and raisinges the question of which equation is better. To clarify the uncertainty and to answer this question, the derivation of T equations in terms of T_s and H_2O-related variables is thoroughly studied. The two equations above were developed with approximations;. Ttherefore, neither of their accuracies wasere evaluated, nor was the question answered. Based on the first principles, this study derives the T equation in terms of T_s and water vapor molar mixing ratio (χ_{H2O}) without any assumption and approximation. Thus, this equation ~~itself does not have any~~ inherently lacks error, and the accuracy in T from this equation (equation-computed T) depends solely on the measurement accuracies of T_s and χ_{H2O}. Based on current specifications for T_s and χ_{H2O} in the CPEC300 series and given their maximized measurement uncertainties, the accuracy in equation-computed T is specified within ±1.01 K. This accuracy uncertainty is propagated mainly (±1.00K) from the uncertainty in T_s measurements and little (±0.02K) from the uncertainty in χ_{H2O} measurements. ~~Apparently, the~~An improvement ~~o~~in measurement technologies, particularly for T_s, would be a key to narrowing this accuracy range. Under normal sensor and weather conditions, the specified accuracy is overestimated in range and actual accuracy is better. Equation-computed T has a frequency response equivalent to high-frequency T_s and is insensitive to solar contamination during measurements. ~~As s~~Synchronized at a temporal scale of measurement frequency and matched at a spatial scale of measurement volume with all aerodynamic and thermodynamic variables, this T has ~~its~~ advanced merits in boundary-layer meteorology and applied meteorology.

Keywords: ~~CO_2 flux, H_2O flux,~~ Air temperature accuracy, high-frequency air temperature, infrared gas analyzer, sonic anemometer, turbulen~~t~~ce air temperature~~measurements~~.

1 Introduction

The equation of state, $P = \rho RT$, is a fundamental equation for describing all atmospheric flows where P is atmospheric pressure, ρ is moist air density, R is gas constant for moist air, and T is air temperature (Wallace and Hobbs, 2006). In ~~the~~ boundary-layer flow, where turbulence is nearly always present, accurate representation of the "state" of the atmosphere at any given "point" and time requires consistent representation of spatial and temporal scales for all thermodynamic factors of P, ρ, and T (Panofsky and Dutton, 1984). Additionally, for observing fluxes describing exchanges of quantities such as heat and moisture between the earth and the atmosphere, it is critical to know all three-dimensional (3-D) components of wind speed at the same location and temporal scale as the thermodynamic variables (Laubach and McNaughton, 1998).

In a closed-path eddy-covariance (CPEC) system, the 3-D wind components and sonic temperature (T_s) are measured by a 3-D sonic anemometer in the sonic measurement volume near which air is sampled through the orifice of an infrared ~~gas~~ H_2O/CO_2 analyzer (hereafter referred as to infrared analyzer) into its closed-path H_2O/CO_2 measurement cuvette where air moisture is measured by the analyzer (Fig. 1). The flow pressure inside the cuvette (P_c) and the differential (ΔP) between P_c and ambient flow pressure in the sampling location are also measured (Campbell Scientific Inc., 2018c). Atmospheric P in the sampling volume, therefore, is a sum of P_c and ΔP. P_c, along with the internal T, is ~~are~~ further used for infrared measurements of air moisture (i.e., ρ_w, H_2O density) to calculate the water mixing ratio (χ_w) inside the cuvette that is also equal to χ_w in the CPEC measurement volume including sonic measurement volume and air sampling location. Finally, the T_s and χ_w from the CPEC measurement volume, after spatial and temporal synchronization (Horst and Lenschow, 2009), are used to calculate the T inside this volume. Two optional equations (Schotanus et al., 1983; Kaimal and Gaynor, 1991; see ~~the s~~Section ~~of~~2 Background), which need rigorous evaluation, are available for this T calculation. In summary, the boundary-layer flow measured by a CPEC system has all variables quantified with consistent representation of spatial and temporal scales for moist turbulence thermodynamics (i.e., state) if the following are available: ~~the~~ 3-D wind; P measured differentially; T from an equation; and ρ from P, T, and χ_w.

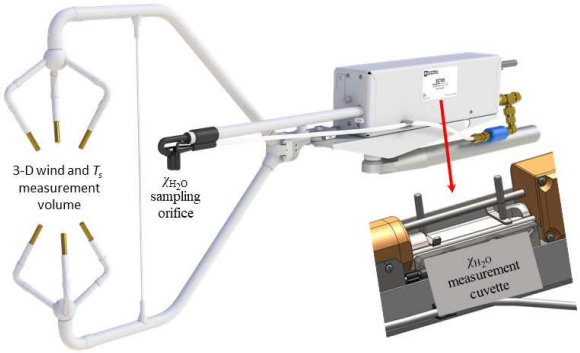

Figure 1: Measurement volume for three-dimensional (3-D) wind and sonic temperature (T_s), sampling orifice for H_2O molar mixing ratio (χ_{H_2O}), and measurement cuvette for χ_{H_2O} in CPEC300 series (Campbell Scientific Inc., UT, USA).

In this paper, ~~we~~the authors 1) derive a T equation in terms of T_s and χ_w based on ~~the~~ first principles as an alternative to the commonly used equations ~~which~~that are based on approximations; 2) estimate and verify the accuracy of the first-principles T; 3) assess the expected advantages of the first-principles T as a high-frequency signal insensitive to solar contamination suffered by~~to~~ conventional T sensor measurements (Lin et al., 2001; Blonquist and Bugbee, 2018)~~,~~; and 4) brief ~~address~~ the potential applications of the derived T equation in flux measurements. We first provide a ~~brief~~ summary of the moist turbulence thermodynamics of the boundary-layer flows measured by CPEC flux systems.

2 Background

A CPEC system is commonly ~~is~~ used to measure boundary-layer flows for the CO_2, H_2O, heat, and momentum fluxes between ecosystems and the atmosphere. Such a system is equipped with a 3-D sonic anemometer to measure the speed of sound in three dimensions in the central open-space of the instrument (here~~in~~after~~,~~ refer to as open-space), from which can be calculated T_s and 3-D components of wind at fast response. Integrated with this sonic anemometer, a fast-response infrared gas analyzer concurrently measures CO_2 and H_2O in its cuvette (closed-space) of infrared measurements, through which air is sampled under pump pressure while being heated (Fig. 1). The analyzer outputs the CO_2 mixing ratio (i.e., $\chi_{CO_2} = \rho_{CO_2}/\rho_d$, ~~-~~where ρ_{CO_2} is CO_2 density and ρ_d is dry air density) and χ_w (i.e., ρ_w/ρ_d). Together, these instruments provide high-frequency (e.g., 10 Hz) measurements from which the fluxes are computed (Aubinet et al., 2012) at a "point" represented by the sampling space of the CPEC system.

These basic high-frequency measurements of 3-D wind speed, T_s, χ_w, and χ_{CO_2} provide observations from which mean and fluctuation properties of air, such as ρ_d, ρ, ρ_w, ρ_{co_2}, and, hence, fluxes can be determined. For instance, water vapor flux is

calculated from $\overline{\rho}_d \overline{w'\chi_w'}$, where w is vertical velocity of air and prime indicates the fluctuation of variable away from its mean as indicated by overbar, (e.g., $w' = w - \overline{w}$). Given the measurements of χ_w and P from CPEC systems, and based on the gas laws (Wallace and Hobbs, 2006), ρ_d is derived from

$$\rho_d = \frac{P}{T\left(R_d + R_v \chi_w\right)} \quad (1)$$

where R_d is gas constant for dry air and R_v is gas constant for water vapor. In turn, ρ_w is equal to $\rho_d \chi_w$ and ρ is a sum of ρ_d and ρ_w. All mentioned physical properties can be derived if T in Eq. (1) for ρ_d is acquired.

Additionally, equations for ecosystem exchange and flux require $\overline{\rho}_d$ (Gu et al., 2012) and $\overline{\rho_d w}$ (Foken et al., 2012). Furthermore, due to accuracy limitations in measurements of w from a modern sonic anemometer, the dry air flux of $\overline{\rho_d w}$ must be derived from $\overline{\rho_d' w'} - \overline{\rho}_d \overline{w}$ (Webb et al., 1980; Lee and Massman, 2011). Because of its role in flux measurements, a high-frequency representation of ρ_d is needed. To acquire such ρ_d from Eq. 1 for advanced applications, high-frequency T in temporal synchronization with χ_w and P is needed.

In a modern CPEC system, P is measured using a fast-response barometer suitable for measurements at a high frequency (e.g., 10 Hz, Campbell Scientific Inc., 2018a) and, as discussed above, χ_w is a high-frequency signal from a fast-response gas analyzer (e.g., commonly up to 20 Hz). If T is measured using a slow-response sensor, the three independent variables in Eq. (1) do not have equivalent synchronicity in frequency response. In terms of frequency response, ρ_d' cannot be correctly aquired. $\overline{\rho}_d$ derived based on Eq. (1) also has uncertainty, although it can be approximated from either of the two following equations:

$$\overline{\rho}_d = \overline{\frac{P}{T\left(R_d + R_v \chi_w\right)}}, \quad (2)$$

and

$$\overline{\rho}_d = \frac{\overline{P}}{\overline{T}\left(R_d + R_v \overline{\chi}_w\right)}. \quad (3)$$

Eq. (2) is mathematically valid in averaging rules (Stull, 1988), but the response of the system to T is slower than to χ_w, and even P, while ~~the~~ Eq. (3) is invalid under averaging rules although its three over-bar independent variables can be evaluated over an average interval. Consequently, neither $\overline{\rho_d w}$ nor $\overline{\rho}_d$ can be evaluated strictly in theory.

Measurements of T at high frequency (similar to those at low-frequency) are contaminated by solar radiation, even under shields (Lin et al., 2001) and when aspirated (Campbell Scientific Inc., 2010; R.M. Young Company, 2004; Apogee Instrument Inc., 2013; Blonquist and Bugbee, 2018). Additionally, the aspiration method cannot acquire T at high frequency due to the disturbance of an aspiration-fan to natural turbulent flows, and fine wires ~~and aspiration methods~~ have limited applicability for long-term measurements in rugged field conditions typically encountered in ecosystem monitoring.

To avoid the issues above in use of either slow- or fast-response T sensors under field conditions, deriving T from T_s and χ_w (Schotanus et al., 1983; Kaimal and Gaynor, 1991) is an advantageous alternative to the applications of T in CPEC measurements and is a significant technology for instrumentation to pursue. In a CPEC system, T_s is measured at a high frequency (e.g., 10 Hz) using a fast-response sonic anemometer to detect the speed of sound in the open-space (Munger et al.,

2012) provided there is no evidence of contaminationed by solar radiation. It is a high-frequency signal. χ_w is measured at the same frequency as for T_s using a gas analyzer equivalent to the sonic anemometer in high-frequency response time (Ma et al., 2017). χ_w reported from a CPEC system is converted from water vapor molar density measured inside the closed-space cuvette whose internal pressure and internal temperature are more stable than P and T in the open-space and can be more accurately measured. Because of this, solar warming and radiation cooling of the cuvette is irrelevant, as long as water molar density, pressure, and temperature inside the closed-space cuvette are more accurately measured. Therefore, it could be reasonably expected that T calculated from T_s and χ_w in a CPEC system should be a high-frequency signal insensitive to solar radiation.

The first of two equations commonly used to compute T from T_s and air moisture-related variables are,is given by Schotanus et al. (1983), as:

$$T = T_s(1+0.51q)^{-1}, \tag{4}$$

where q is specific humidity, defined as a ratio of water vapor to moist air density., and The second equation is given by Kaimal and Gaynor (1991), as:

$$T = T_s\left(1+0.32\frac{e}{P}\right)^{-1}, \tag{5}$$

where e is water vapor pressure. Re-arranging these two equations gives T in terms of T_s and χ_w. Expressing q in terms of ρ_d and ρ_w, Eq. (4) becomes

$$T = T_s\left(1+0.51\frac{\rho_w}{\rho_d+\rho_w}\right)^{-1} = T_s\left(1+0.51\frac{\chi_w}{1+\chi_w}\right)^{-1}, \tag{6}$$

and expressing e and P using the equation of state, Eq. (5) becomes

$$T = T_s\left(1+0.32\frac{R_v T\rho_w}{R_d T\rho_d + R_v T\rho_w}\right)^{-1} = T_s\left(1+0.51\frac{\chi_w}{1+1.61\chi_w}\right)^{-1}. \tag{7}$$

The χ_w-related terms in the denominator inside parentheses in both equations above clearly reveal that T values from the same T_s and χ_w using the two commonly used Eqs. (4) and (5) will not be the same. The absolute difference in the values ([ΔT_e, i.e., the difference in T between Eqs. (4) and (5)] can be analytically expressed as:

$$\Delta T_e = \frac{0.31 T_s \chi_w^2}{1+3.63\chi_w+3.20\chi_w^2}. \tag{8}$$

Given that, in a CPEC system, the sonic anemometer has an operational range in T_s of -30 to 57 °C (Campbell Scientific Inc., 2018b) and a gas analyzer has a measurement range in χ_w of 0 to 0.045 $kgH_2O\ kg^{-1}$ (Campbell Scientific Inc., 2018a), ΔT_e ranges up to 0.177 K, which brings an uncertainty in accuracy of T calculated from either Eq. (4) or (5) and raises the question of which equation is better.

Reviewing the sources of Eq. (4) (Schotanus et al., 1983; Swiatek, 2009; van Dijk, 2002) and Eq. (5) (Ishii, 1932; Barrett and Suomi, 1949; Kaimal and Businger, 1963; Kaimal and Gaynor, 1991), it was found that approximation procedures were used in derivation of both equations, but the approach to the derivation of Eq. (4) (Appendix A) is different from that of Eq. (5) (Appendix B). These different approaches create a differencedisparity between the two commonly used equations as shown in Eq. (8), and the approximation procedures lead to the controversy as to which equation is more accurate. The controversy can be avoided if the T equation in terms of T_s and χ_w can be derived from the T_s equation and the first-principles equations, if possible,

without an approximation and verified against precision measurements of T with minimized solar contamination.

3 Theory ~~Derivation of air temperature equation~~

As discussed above, a sonic anemometer measures the speed of sound (c) concurrently with measurement of the 3-D wind speed (Munger et al., 2012). The speed of sound in the homogeneous atmospheric boundary-layer is defined by Barrett and Suomi (1949) as:

$$c^2 = \gamma \frac{P}{\rho}, \tag{9}$$

where γ is the ratio of moist air specific heat at constant pressure (C_p) to moist air specific heat at constant volume (C_v). Substitution of the equation of state into Eq. (9)~~,~~ gives T as a function of c:

$$T = \frac{c^2}{\gamma R}. \tag{10}$$

This equation reveals the opportunity to use measured c for the T calculation; however, both γ and R depend on air humidity, which is unmeasurable by ~~a~~ sonic anemometry itself; Eq. (10) is, therefore, not applicable for T calculations inside a sonic anemometer. Alternatively, γ is replaced with its counterpart for dry air [γ_d, 1.4003, i.e., the ratio of dry air specific heat at constant pressure (C_{pd}, 1,004 J K^{-1} kg^{-1}) to dry air specific heat at constant volume (C_{vd}, 717 J K^{-1} kg^{-1})] and R is replaced with its counterpart for dry air (R_d, 287.06 J K^{-1} kg^{-1}, i.e., gas constant for dry air). Both replacements make the right side of Eq. (10) become $c^2/\gamma_d R_d$ which is no longer a measure of T. However, γ_d and R_d are close to their respective values of γ and R in magnitude, and, after the replacements, the right side of Eq. (10) ~~after the replacements~~ is defined as sonic temperature (T_s), given by (Campbell Scientific Inc., 2018b):

$$T_s = \frac{c^2}{\gamma_d R_d}. \tag{11}$$

Comparing this equation to Eq. (10), given c, if air is dry, T must be equal to T_s; therefore, the authors ~~we~~ define taht "*sonic temperature of moist air is the temperature that its dry air component reaches when moist air has the same enthalpy*"~~.~~" Since both γ_d and R_d are constants and c is measured by a sonic anemometer and corrected for crosswind effect inside the sonic anemometer based on its 3-D wind measurements (Liu et al., 2001; Zhou et al., 2018), Eq. (11) is used inside the operating system of modern sonic anemometers to report T_s instead of T.

Equations (9) to (11) provide a theoretical basis of first principles to derive the relationship of T to T_s and χ_w. In Eq. (9), γ and ρ vary with air humidity and P is related to ρ as described by the equation of state. Consequently, the derivation of T from T_s and χ_w for CPEC systems needs to address the relationship of γ, ρ, and P to air humidity in terms of χ_w.

3.1 Relationship of γ to χ_w

For moist air, the ratio of specific heat at constant pressure to specific heat at constant volume is:

$$\gamma = \frac{C_p}{C_v}, \tag{12}$$

where C_p varies with air moisture between C_{pd} and C_{pw} (water vapor specific heat at constant pressure, 1,952 J kg^{-1} K^{-1}). It is the arithmetical average of C_{pd} and C_{pw} weighted by dry air mass and water vapor mass, respectively, given by (Stull, 1988; Swiatek,

2009):

$$C_p = \frac{C_{pd}\rho_d + C_{pw}\rho_w}{\rho_d + \rho_w}. \quad (13)$$

Based on the same rationale, C_v is:

$$C_v = \frac{C_{vd}\rho_d + C_{vw}\rho_w}{\rho_d + \rho_w}, \quad (14)$$

where C_{vw} is the specific heat of water vapor at constant volume (1,463 J kg^{-1} K^{-1}). Substituting Eqs. (13) and (14) into Eq. (12) generates:

$$\gamma = \gamma_d \frac{1+\left(C_{pw}/C_{pd}\right)\chi_w}{1+\left(C_{vw}/C_{vd}\right)\chi_w}. \quad (15)$$

3.2 Relationship of P/ρ to χ_w

Atmospheric P is the sum of P_d and e. Similarly, ρ is the sum of ρ_d and ρ_w. Using the equation of state, the ratio of P to ρ can be expressed as:

$$\frac{P}{\rho} = \frac{R_d T\rho_d + R_v T\rho_w}{\rho_d + \rho_w} = \frac{R_d T\left(1+\frac{R_v}{R_d}\chi_w\right)}{1+\chi_w}. \quad (16)$$

In this equation, the ratio of R_v to R_d is given by:

$$\frac{R_v}{R_d} = \frac{R^*/M_w}{R^*/M_d} = \frac{1}{M_w/M_d}, \quad (17)$$

where R^* is the universal gas constant, M_w is the molecular mass of water vapor (18.0153 kg kmol^{-1}), and M_d is the molecular mass of dry air (28.9645 kg kmol^{-1}). The ratio of M_w to M_d is 0.622, conventionally denoted by ε. Substituting Eq. (17), after its denominator is represented by ε, into Eq. (16) leads to:

$$\frac{P}{\rho} = \frac{R_d T(\varepsilon+\chi_w)}{\varepsilon(1+\chi_w)}. \quad (18)$$

3.3 Relationship of T_s to T and χ_w

Substituting Eqs. (15) and (18) into Eq. (9), c^2 is expressed in terms of T and χ_w along with atmospheric physics constants~~: Further, substituting c^2 into Eq. (11) generates:~~

$$c^2 = \frac{R_d\gamma_d T(\varepsilon+\chi_w)\left[1+\left(C_{pw}/C_{pd}\right)\chi_w\right]}{\varepsilon(1+\chi_w)\left[1+\left(C_{vw}/C_{vd}\right)\chi_w\right]} \quad (19)$$

Further, substituting c^2 into Eq. (11) generates:

$$T_s = T\frac{(\varepsilon+\chi_w)\left[1+\left(C_{pw}/C_{pd}\right)\chi_w\right]}{\varepsilon(1+\chi_w)\left[1+\left(C_{vw}/C_{vd}\right)\chi_w\right]}. \quad (20)$$

~~Now, t~~This equation (20) now expresses T_s in terms of T of interest to this study, χ_w measured in CPEC systems, and atmospheric

physics constants (i.e., ε, C_{pw}, C_{pd}, C_{vw}, and C_{vd}).

3.4 Air temperature equation

Rearranging the terms in Eq. (20) results in

$$T = T_s \frac{\varepsilon(1+\chi_w)\left[1+\left(C_{vw}/C_{vd}\right)\chi_w\right]}{\left(\varepsilon+\chi_w\right)\left[1+\left(C_{pw}/C_{pd}\right)\chi_w\right]} \tag{21}$$

This equation shows that T is a function of T_s and χ_w that are measured at high frequency in a CPEC system by a sonic anemometer and an infrared analyzer.

A CPEC system outputs water vapor molar mixing ratio (Campbell Scientific Inc., 2018a) commonly used in the community of eddy-covariance fluxes (AmeriFlux, 2018). The relation of water vapor mass to molar mixing ratio (χ_{H_2O} in molH_2O mol^{-1}) is given by:

$$\chi_w = \frac{M_w}{M_d}\chi_{H_2O} = \varepsilon\chi_{H_2O}. \tag{22}$$

Substituting this relation into Eq. (21) and denoting Cvw/Cvd with γ_v = 2.04045 and C_{pw}/C_{pd} with γ_p = 1.94422, Eq. (21) is expressed as:

$$T = T_s \frac{\left(1+\varepsilon\chi_{H_2O}\right)\left(1+\varepsilon\gamma_v\chi_{H_2O}\right)}{\left(1+\chi_{H_2O}\right)\left(1+\varepsilon\gamma_p\chi_{H_2O}\right)}. \tag{23}$$

This is the air temperature equation in terms of T_s and χ_{H_2O} for use in CPEC systems. It is derived from a theoretical basis of first principles [i.e., Eqs. (9) to (11)]. In its derivation, except for the use of the equation of state and Dalton's law, no other assumptions nor approximations are used. Therefore, Eq. (23) is an exact equation of T in terms of T_s and χ_{H_2O} for the turbulent air flow sampled through a CPEC system and thus avoids the controversy in use of Eqs. (4) and (5) arising from approximations as shown in Appendices A and B. Therefore, T computed from this equation (hereinafter referred to as equation-computed T) should be accurate as long as the values of T_s and χ_{H_2O} are exact.

For this study, however, T_s and χ_{H_2O} are measured by the CPEC systems deployed in the field under changing weather conditions through four seasons. Their measured values must include measurement uncertainty in T_s, denoted by ΔT_s and in χ_{H_2O} as well, denoted by $\Delta\chi_{H_2O}$. The uncertainties, ΔT_s and/or $\Delta\chi_{H_2O}$, unavoidably propagate to create uncertainty in equation-computed T, denoted by ΔT, which makes an exact T impossible. In numerical analysis (Burden and Faires, 1993) or in statistics (Snedecor and Cochran, 1991), any applicable equation requires the specification of an uncertainty term. Therefore, the equations for T should include specification of their respective uncertainty expressed as the bounds (i.e., the maximum and minimum limits) specifying the range of the equation-computed T that need to be known for any application. According to the definition of accuracy that was advanced by the International Organization for Standardization (2012), this uncertainty range is equivalent to the "accuracy" asof the range contributed by both systematic errors (trueness) and random variability (precision). Apparently, ΔT_s is the accuracy of T_s measurements and $\Delta\chi_{H_2O}$ is the accuracy of χ_{H_2O} measurements. Both should be evaluated from their measurement uncertainties, respectively. The accuracy of equation-computed T is ΔT. It should be specified through its relationship to ΔT_s and $\Delta\chi_{H_2O}$.

3.5 Relationship of ΔT to ΔT_s and $\Delta\chi_{H_2O}$

As measurement accuracies, ΔT_s and $\Delta\chi_{H_2O}$ can be reasonably considered as small increments in a calculus sense. As such, depending on both small increments, ΔT is the total differential of T with respect to T_s and χ_{H_2O}, given by:

$$\Delta T = \frac{\partial T}{\partial T_s}\Delta T_s + \frac{\partial T}{\partial \chi_{H_2O}}\Delta\chi_{H_2O} \tag{24}$$

The two partial derivatives in the right side of this equation can be derived from Eq. (23). Substituting the two partial derivatives into this equation leads to

$$\Delta T = \frac{T}{T_s}\Delta T_s + T\left[\frac{\varepsilon+\varepsilon\gamma_v\left(1+2\varepsilon\chi_{H_2O}\right)}{\left(1+\varepsilon\chi_{H_2O}\right)\left(1+\varepsilon\gamma_v\chi_{H_2O}\right)} - \frac{1+\varepsilon\gamma_p\left(1+2\chi_{H_2O}\right)}{\left(1+\chi_{H_2O}\right)\left(1+\varepsilon\gamma_p\chi_{H_2O}\right)}\right]\Delta\chi_{H_2O} \tag{25}$$

This equation indicates that in dry air when $T = T_s$, ΔT is equal to ΔT_s if χ_{H_2O} is measured accurately (i.e., $\Delta\chi_{H_2O} = 0$ while $\chi_{H_2O} = 0$). However, air in the atmospheric boundary-layer where CPEC systems are used is always moist. Given this equation, ΔT at T_s and χ_{H_2O} can be evaluated by using ΔT_s and $\Delta\chi_{H_2O}$, both of which are related to the measurement specifications of sonic anemometers for T_s (Campbell Scientific Inc., 2018b) and of infrared analyzers for χ_{H_2O} (Campbell Scientific Inc., 2018a). Sonic anemometers and infrared analyzers with different models and brands have different specifications from their manufacturers. Any combination of sonic and infrared instruments has a combination of the ΔT_s and $\Delta\chi_{H_2O}$ that are specified by their manufacturers. In turn, from Eq. (25), the combination generates ΔT of equation-computed T for the corresponding combination of the sonic and infrared instruments with given models and brands. Therefore, Eqs. (23) and (25) are applicable to any CPEC system beyond our study brand.

In the right side of Eq. (25), the first term with ΔT_s can be expressed as ΔT_{T_s} (i.e., uncertainty portion of ΔT due to ΔT_s) and the second term with $\Delta\chi_{H_2O}$ can be expressed as $\Delta T_{\chi_{H_2O}}$ (i.e., uncertainty portion of ΔT due to $\Delta\chi_{H_2O}$). Using ΔT_{T_s} and $\Delta T_{\chi_{H_2O}}$, this equation can be simplified as:

$$\Delta T = \Delta T_{T_s} + \Delta T_{\chi_{H_2O}} \tag{26}$$

Assessment on the accuracy of equation-computed T is to evaluate ΔT_{T_s} and $\Delta T_{\chi_{H_2O}}$ correspondingly from ΔT_s and $\Delta\chi_{H_2O}$.

4 Accuracy ~~of equation-computed T~~

The CPEC system for this study is CPEC310 (Campbell Scientific Inc., ~~Logan,~~ UT, USA)~~,~~ ~~including~~ whose major components are a CSAT3A sonic anemometer (updated version in 2016) for fast response to 3-D wind and T_s and an EC155 infrared analyzer for fast response to H_2O along with CO_2 (Burgon et al., 2015; Ma et al., 2017). The system operates in a T range of -30 to 50 °C and measures χ_{H_2O} in a range up to 79 mmolH_2O mol^{-1} (i.e., 37 °C dew point temperature at 86 kPa under manufacturer environment); therefore, the accuracy of equation-computed T, depending on ΔT_s and $\Delta\chi_{H_2O}$, should be defined and estimated in a domain over both ranges.

4.1 ΔT_s (~~m~~Measurement accuracy in T_s)

As is true for other sonic anemometers (e.g., Gill Instruments, 2004), the CSAT3A has not been assigned a T_s measurement performance (Campbell Scientific Inc., 2018b) because the theories and methodologies of how to specify this performance, to the

best of our knowledge, have not been clearly defined. The performance of the CSAT series for T_s is best near production temperature around 20 °C and drifts little away from this temperature. Within the operational range of a CPEC system in ambient air temperature, the updated version of CSAT3A has an overall uncertainty to be ±~~–~~1.00 °C (i.e., $|\Delta T_s| < 1.0$ K, vis personal communication with CSAT authority: Larry Jacobsen through email in 2017 and in ~~his office~~ person in 2018).

4.2 $\Delta\chi_{H_2O}$ (~~m~~Measurement accuracy in χ_{H_2O})

The accuracy in H_2O measurements from infrared analyzers~~,~~ depends~~ing on~~ upon analyzer measurement performance. This performace is specified using four component uncertainties: 1) precision variability (σ_{H_2O}), 2) maximum zero drift range with ambient air temperature (d_{wz}), 3) maximum gain drift with ambient air temperature ($\pm\delta_{H_2O}\chi_{H_2O}$ where δ_{H_2O} is gain drift percentage), and 4) cross-sensitivity to CO_2 (s_c) (LI-COR Biosciences, 2016; Campbell Scientific Inc., 2018c). Zhou et al. (2021) composited the four component uncertainties as an accuracy model formulated as the H_2O accuracy equation for CPEC systems applied in ecosystems, given by:

$$\Delta\chi_{H_2O} = \pm\left[1.96\sigma_{H_2O} + 585|s_c| + \frac{|d_{wz}| + \delta_{H_2O\_g}\chi_{H_2O}}{T_{rh} - T_{rl}} \times \begin{cases} T_c - T & T_c > T > T_{rl} \\ T - T_c & T_c < T < T_{rh} \end{cases}\right], \quad (27)$$

where T_c is ambient air temperature at which an infrared analyzer was calibrated by the manufacturer to fit its working equation or zeroed/spanned in the field to adjust the zero/gain drift; subscripts *rh* and *rl* indicate the range highest and range lowest values, respectively; and T_{rh} and T_{rl} are the highest- and ~~the~~ lowest-T, respectively, over the operational range of CPEC systems in T. Given the infrared analyzer specifications: σ_{H_2O}, s_c, d_{wz}, $\delta_{H_2O\_g}$, T_{rl} and T_{rh}, this equation can be used to estimate $\Delta\chi_{H_2O}$ in Eq. (25) and eventually for $\Delta T_{\chi_{H_2O}}$ in Eq. (26) over the domain of T and χ_{H_2O}.

4.3 ΔT (Accuracy of equation-computed T)

The accuracy of equation-computed T can be evaluated using ΔT_s and $\Delta\chi_{H_2O}$ (Eq. 25), varying with T, T_s, and χ_{H_2O}. Both T and T_s reflect air temperature, being associated with each other through χ_{H_2O} (Eq. 23). Given χ_{H_2O}, T can be calculated from T_s, and vice versa; therefore, for the figure presentations in this study, it is sufficient to use either T or T_s, instead of both, to show ΔT with air temperature. Considering T to be of interest to this study, T will ~~should~~ be used. As such, ΔT can be analyzed over a domain of T and χ_{H_2O} within the operational range of CPEC systems in T from -30 to 50 °C across the analyzer measurement range of χ_{H_2O} from 0 to 0.079 molH_2O mol^{-1}.

To visualize the relationship of ΔT with T and χ_{H_2O}, ΔT is presented better as ordinate along T as abscissa associated with χ_{H_2O}. However, due to the positive dependence of air water vapor saturation on T (Wallace and Hobbs, 2006), χ_{H_2O} has a possible range wider at higher T and narrower at lower T. To present ΔT over the same measure of air moisture even at different T, the saturation water vapor pressure is used to scale air moisture to 0, 20, 40, 60, 80 and 100 (i.e., RH, relative humidity in %). For each scaled RH value, χ_{H_2O} can be calculated at different T and P (Appendix C) for use ~~of~~in Eq. (25). In this way, over the range of T, the trend of ΔT due to each measurement uncertainty source can be shown along the curves with equal RH as the measure of air moisture (Fig. 2).

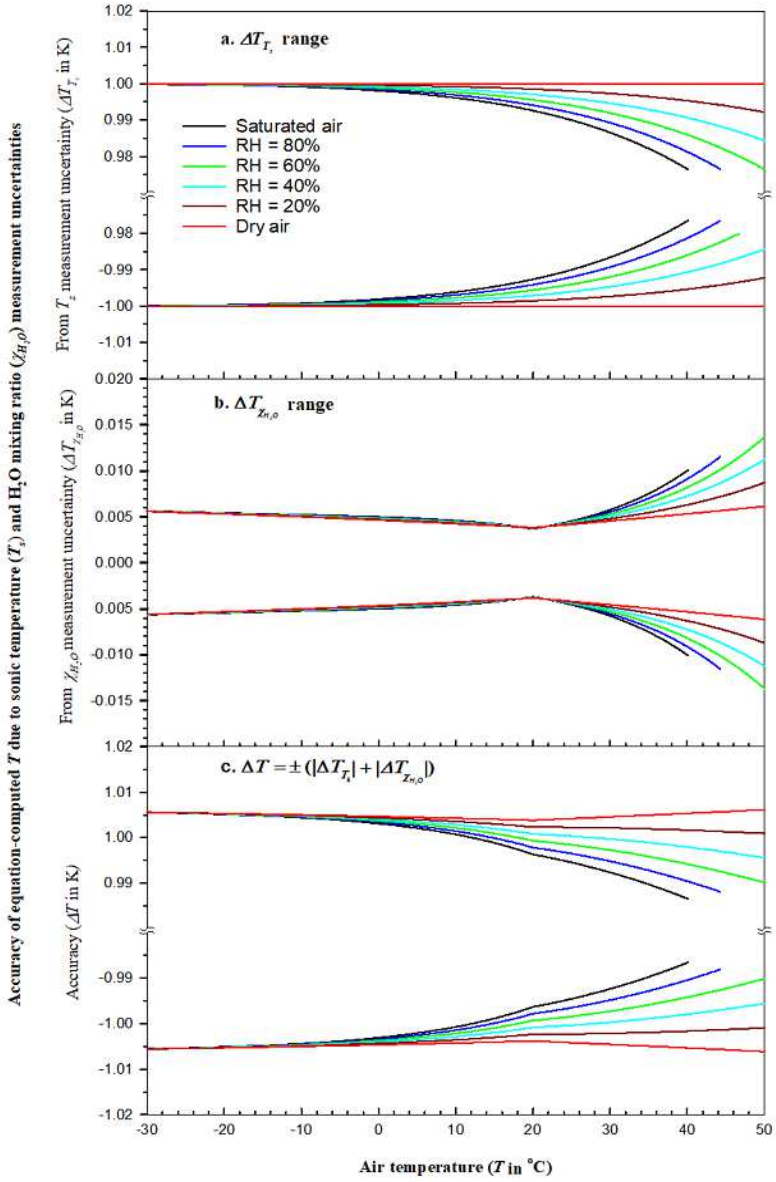

Figure 2: Accuracy of air temperature computed from Eq. (23) (equation-computed *T*) over the measurement range of H_2O molar mixing ratio (χ_{H_2O}) within the operational range of *T* for CPEC300 series (Campbell Scientific Inc., UT, USA); a. Accuracy component of equation-computed *T* due to sonic temperature (T_s) measurement uncertainty; b. Accuracy component of equation-computed *T* due to χ_{H_2O} ~~H_2O mixing ratio~~ measurement uncertainty, and c. ~~the o~~Overall accuracy of equation-computed *T*.

4.3.1 ΔT_{T_s} (Uncertainty portion of ΔT due to ΔT_s)

Given ΔT_s = ±1.00 K and T_s from the algorithm in Appendix C, ΔT_{T_s} in Eq. (26) was calculated over the domain of T and χ_{H2O} (Fig. 2a). Over the whole T range, the ΔT_{T_s} limits range ±1.00 K, becoming a little narrower with χ_{H2O} increasing due to decrease, at the same T_s, in the magnitude T/T_s in Eq. (25). The narrowest limits of ΔT_{T_s}, in an absolute value, varies < 0.01 K over the range of T below 20 °C although > 0.01 K but < 0.03 K above 20 °C, ~~but < 0.03 K~~.

4.3.2 $\Delta T_{\chi_{H2O}}$ (Uncertainty portion of ΔT due to $\Delta \chi_{H2O}$)

Given χ_{H2O} from the algorithm in Appendix C and $\Delta \chi_{H2O}$ from Eq. (27), $\Delta T_{\chi_{H2O}}$ was calculated over the domain of T and χ_{H2O} (Fig. 2b). The parameters in Eq. (27) are given through the specifications of the CPEC300 series ~~(~~[Campbell Scientific Inc., 2018a; 2018c. σ_{H_2O} is 6.0×10^{-6} molH_2O mol^{-1} where mol is a unit for dry air; d_{wz}, $\pm5.0\times10^{-5}$ molH_2O mol^{-1} ~~with T~~; δ_{H2O_g}, 0.30% ~~with T~~; s_c, $\pm5.0\times10^{-8}$ molH_2O mol^{-1} (μmolCO_2 mol^{-1})$^{-1}$; T_c, 20 ºC as Normal Temperature (Wright et al., 2003); T_{rl}, -30 ºC; and T_{rh}, 50 ºC]~~)~~.

As shown in Fig. 2b, $\Delta T_{\chi_{H2O}}$ tends to be smallest at $T = T_c$. However, away from T_c, its range non-linearly becomes wider, very gradually widening below T_c but widening more abruptly above, because, as temperature increases, χ_{H2O} at the same RH increases exponentially (Eqs. (c1) and (c5) in Appendix C) while $\Delta \chi_{H2O}$ increases linearly with χ_{H2O} in Eq. (27). This non-linear range can be summarized to be ±0.01 K below 30 °C and ±0.02 K above 30 °C. Compared to ΔT_{T_s}, $\Delta T_{\chi_{H2O}}$ is much smaller at two orders. ΔT_{T_s} is a large compoonent in ΔT.

4.3.3 ΔT (Combined uncertainty as the accuracy in equation-computed T)

Equation (26) is used to determine the maximum combined uncertainty in equation-computed T for the same RH grade in Fig. 2 by adding together the same sign (i.e., +/-) curve data of ΔT_{T_s} in ~~panel~~Fig. 2a and $\Delta T_{\chi_{H2O}}$ in ~~panel~~Fig. 2b. ΔT ranges at different RH grades are shown in ~~panel~~Fig. 2c. ~~This panel~~ Figure 2c can specifiesy the accuracy of equation-computed T at 101.325 kPa [i.e., Normal Atmospheric Pressure as used by Wright et al. (2003)] over the χ_{H2O} measurement range to be within ±1.02 K. This accuracy for high-frequency T currently is the best in turbulent flux measurement because ±1.00 K is the best in accuracy of T_s from the individual sonic anemometers which are widely used for sensible heat flux in almost all CPEC systems.

4.4 Accuracy of equation-computed T from CPEC field measurements

Equation (23) is derived particularly for CPEC systems in which T_s and χ_{H2O} are measured neither at the same volume nor at the same time. Both variables are measured separately using a sonic anemometer and an infrared analyzer in a spatial separation between the T_s measurement center and the χ_{H2O} measurement cuvette (e.g., Fig. 1), along with a temporal lag in the measurement of χ_{H2O} relative to T_s due to the transport time and phase shift (Ibrom et al., 2007) of turbulent air flows sampled for χ_{H2O} through the sampling orifice to the measurement cuvette (Fig. 3).

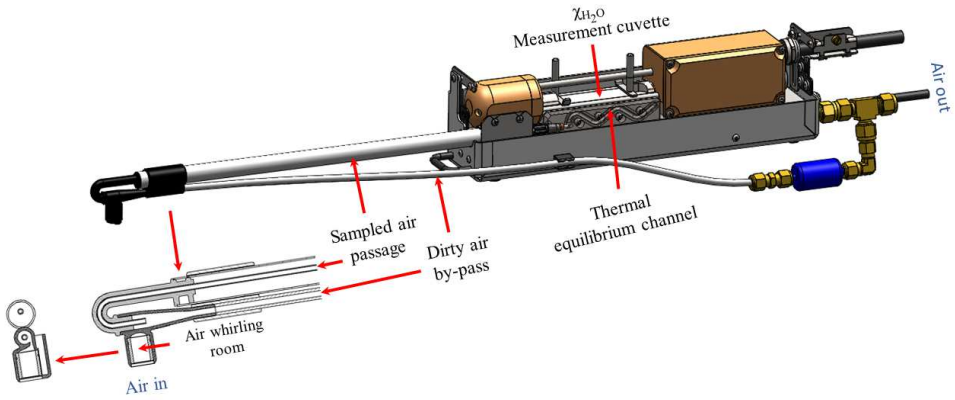

Figure 3: Vortex intake system for air flow through its individual compartments: Air whirling room (2.200 mL), sampled air passage (1.889 mL), thermal equilibrium channel (0.587 mL), and χ_{H2O} measurement cuvette (5.887 mL). The internal space of all compartments adds up to a total volume of 10.563 mL.

Fortunately, the spatial separation scale is ~~at~~ the tens of centimeters ~~scale~~ and the temporal lag scale is of the tens of milliseconds ~~scale~~. In eddy-covariance flux measurements, such a separation misses some covariance signals at higher frequency, which is correctable (Moore, 1986), and such a lag diminishes the covariance correlation, which is recoverable (Ibrom et al., 2007). How such a separation along with the lag influences the accuracy of Eq. (23), as shown in Fig. 2, needs testing against precision measurements of air temperature. The two advantages of the equation-computed *T* discussed in the introduction, namely the fast response to high-frequency signals and the insensitivity to solar contamination in measurements, were studied and assessed during testing when a CPEC system was set up in the Campbell Scientific Instrument Test Field (41.8° N, 111.9° W, 1,360 m asl, UT, USA).

5 Materials and Methods

5.1 Field test station

A CPEC310 system was set as ~~a~~the core of the station in 2018. Beyond its major components briefly described in Section 4, the system also included a barometer (Model: MPXAZ6115A, Freescale Semiconductor, TX, USA) for flow pressure, pump module (SN: 1001) for air sampling, valve module (SN: 1003) to control flows for auto zero/span CO_2 and H_2O, scrub module (SN: 1002) to generate zero gas (i.e., without CO_2 and H_2O) for auto zero procedure, a CO_2 cylinder for CO_2 span, and an EC100 electronic module (SN: 1002, OS: Rev 07.01) to control and measure a CSAT3A, EC155, and ~~a~~ barometer. In turn, the EC100 was connected to, and instructed by, a central CR6 Datalogger (SN: 2981, OS 04) for ~~these~~ sensor measurements, data processing, and data output. In addition to receiving the data output from the EC100, the CR6 also controlled the pump, valve, and scrub modules and measured other micrometeorological sensors in support of ~~for~~ this study.

The micrometeorological sensors included a LI200 pyranometer (SN: 18854, LI-COR~~or~~ Biosciences, ~~Lincoln,~~ NE, USA) to monitor incoming solar radiation, a precision platinum resistance temperature detector (RTD, model 41342, SN: TS25360) inside a fan-aspirated radiation shield (model: 43502, R.M. Young Company, ~~Traverse City,~~ MI, USA) to more accurately measure the T considered with minimized solar contamination due to higher fan-aspiration efficiency, and a HMP155A temperature and humidity sensor (SN: 1073, Vaisala Corporation, Helsinki, Finland) inside a 14-plate wind-aspirated radiation shield ~~of~~ (model 41005) to measure the T under conditions of potentially significant solar contamination during the day due to low wind-aspiration efficiency. The sensing centers of all sensors related to T_s, T, and RH were set at a height of 2.57 m above ~~the~~ ground level. The land surface was covered by natural prairie with a grass height of 5 to 35 cm.

A CR6, supported by EasyFlux-DL ~~–~~CR6CP (Revised version for this study, Campbell Scientific Inc. UT, USA), controlled and sampled the EC100 at 20 Hz. For spectral analysis, the EC100 filtered the data of T_s and χ_{H_2O} for anti-aliasing using a finite impulse response filter with a 0-to-10 Hz (Nyquist folding frequency) passing band (Saramäki, 1993). The EC155 was zeroed for CO_2/H_2O and spanned for CO_2 automatically every other day and spanned for H_2O monthly using a LI-610 Portable Dew Point Generator (LI-COR~~or~~ Biosciences, ~~Lincoln,~~ NE, USA). The LI200, RTD~~T~~, and HMP155A sampled at 1 Hz because of their slow response and the fact that only their measurement means were of interest to this study.

The purpose of this station was to measure the eddy-covariance fluxes to determine turbulent transfers in the boundary-layer flows. The air temperature equation ~~(~~[i.e., Eq. (23)] was developed for T of the turbulent air flows sampled through the CPEC systems. Therefore, this equation can be tested based on how the CPEC310 measures the boundary-layer flows related to turbulent transfer.

5.2 ~~6~~ Turbulent transfer and CPEC310 measurement

In atmospheric boundary-layer flows, air constituents along with heat and momentum (i.e., air properties) are transferred dominantly by individual turbulent flow eddies with various sizes (Kaimal and Finnigan, 1994). Any air property is considered as more homogenous inside each smaller eddy and as more heterogenous among larger eddies (Stull, 1988). Due to this heterogeneity, an eddy in motion among others is transferring air properties to its surroundings. Therefore, to measure the transfer in amount and direction, a CPEC system was designed to capture T_s, χ_{H_2O}, and 3-D flow speeds from individual eddies. Ideal measurements should be fast enough to capture, although ~~even~~ impossible, all eddies with different sizes through the measurement volume and sampling orifice of the CPEC system (Fig. 1). To capture more eddies, ~~with~~of as many sizes as possible, the CPEC measurements were set at a high frequency (20 Hz in this study) because, given 3-D speeds, the smaller the~~an~~ eddy, the shorter time the said eddy takes to pass the sensor measurement volume.

Ideally, each measurement captures an individual eddy for all variables of interest so that the measured values are representative of this eddy. So, for instance, in our effort ~~case~~ to compute T from a pair of T_s and χ_{H_2O}, the pair simultaneously measured from the same eddy could better reflect its T at the measurement time; however, in a CPEC system, T_s and χ_{H_2O} are measured with separation in both space (Fig. 1) and time (Fig. 3).

If an eddy passing the sonic anemometer is significantly larger than the dimension of separation between the T_s measurement volume and the χ_{H_2O} sampling orifice (Fig. 1), the eddy is instantaneously measured for its 3-D wind and T_s in the volume while also sampled in~~to~~ the orifice for χ_{H_2O} measurements. However, if the eddy is smaller and flows along the alignment of separation, the sampling takes place either a little earlier or later than the measurement~~,~~ (e.g., earlier if T_s is measured later, and vice versa). However, depending on its size, an eddy flowing beyond the alignment from other directions, although measured by the sonic

anemometer, may be missed by the sampling orifice passed by other eddies and, in other cases, although sampled by the orifice, may be missed by the measurement of the sonic anemometer.

Additionally, the air flow sampled for χ_{H2O} measurements is not measured at its sampling time on the sampling orifice, but instead is measured, in lag, inside the χ_{H2O} measurement cuvette (Fig. 3). The lag depends on the time needed for the sampled flow to travel through the CPEC sampling system (Fig. 3). Therefore, for the computation of T, χ_{H2O} is better synchronized and matched with T_s as if simultaneously measured from the same eddy.

5.3 ~~7~~ Temporal synchronization and spatial match for T_s with χ_{H2O}

In the CPEC310 system, a pair of T_s and χ_{H2O} that were received by CR6 from EC100 in one data record (i.e., data row) were synchronously measured, through Synchronous Device for Measurement Communication Protocol (Campbell Scientific Inc., 2018c), ~~at the same time~~ in the T_s measurement volume and χ_{H2O} measurement cuvette (Fig. 1). Accordingly, within one data row of time series received by CR6, χ_{H2O} was sampled earlier than T_s was measured. As discussed above, T_s and χ_{H2O} in the same row, although measured at the same time, might be not measured ~~not~~ from the same eddy ~~although measured at the same time~~. If so, the χ_{H2O} measurement from the same eddy of this T_s might occur in another data row, and vice versa. In any case, a logical procedure for ~~the~~ a synchronized~~ation~~ match is first to pair T_s with χ_{H2O} programmatically in CR6, as the former was measured at the same time as the latter was sampled.

5.3.1 ~~7.1~~ Synchronize T_s measured to χ_{H2O} sampled at the same time

Among the rows in time series received by CR6, any two consecutive rows were measured sequentially at a fixed time interval (i.e., measurement interval). Accordingly, anemometer data in any data row can be synchronized with analyzer data in a later row from the eddy sampled by the analyzer sampling orifice at the measurement time of the sonic anemometer. How many rows later depends on the measurement interval and the time length of the analyzer sample from its sampling orifice to the measurement cuvette. The measurement interval commonly is 50 or 100 ms for a 20- or 10-Hz measurement frequency, respectively. The time length is determined by the internal space volume of sampling system (Fig. 3) and the flow rate of sampled air driven by a diaphragm pump (Campbell Scientific Inc., 2018a).

As shown in Fig. 3, the total internal space is 10.563 mL. The rate of sampled air through the sampling system nominally is 6.0 L min^{-1} at which the sampled air takes 106 ms to travel from the analyzer sampling orifice to the cuvette exhaust outlet (Fig. 3). Given that the internal optical volume inside the cuvette is 5.887 mL, the air in the cuvette was sampled ~~in~~ during a period of 47 to 106 ms earlier. Accordingly, anemometer data in a current row of time series should be synchronized with analyzer data in the next row for 10-Hz data and, for 20-Hz data, the row after that ~~following next one~~. After synchronization, the CR6 stores anemometer and analyzer data in a synchronized matrix (variables unrelated to this study were omitted) as a time series:

$$\begin{bmatrix} \cdots\cdots\cdots \\ u(t_i) \;\; v(t_i) \;\; w(t_i) \;\; T_s(t_i) \;\; d_s(t_i) \;\; \chi_{H_2O}(t_i) \;\; d_g(t_i) \;\; s(t_i) \\ \cdots\cdots\cdots \end{bmatrix}, \tag{28}$$

where u and v are horizontal wind speeds orthogonal to each other; w is vertical wind speed; d_s and d_g are diagnosis codes for sonic anemometer and infrared gas analyzer, respectively; s is analyzer signal strength ~~of gas analyzer~~ for H_2O; t is time and its subscript i is its index; and the difference between t_i and t_{i+1} is a measurement interval ($\Delta t = t_{i+1} - t_i$). In any row of matrix (28)

(e.g., the *i*th row), t_i for anemometer data is the measurement time plus instrument lag and t_i for analyzer data is the sampling time plus the same lag. The instrument lag is defined as the number of measurement intervals used for data processing inside EC100 after the measurement and subsequent data communication to CR6. Regardless of instrument lag, T_s and χ_{H2O} in each row of synchronization matrix were temporally synchronized as measured and sampled at the same time.

5.3.2 ~~7.2~~ Match T_s measured to χ_{H2O} sampled from the same eddy

As discussed in Section 5.2~~6~~, at either T_s measurement or χ_{H2O} sampling time, if an eddy ~~was~~is large enough to enclose both T_s measurement volume and χ_{H2O} sampling orifice (Fig. 1), T_s and χ_{H2O} in the same row of synchronization matrix (28) belong to the same eddy~~;~~, otherwise, they belong to different ~~one~~eddies. For any eddy size, it would be ideal if T_s could be spatially matched with χ_{H2O} as a pair for the same eddy; however, this match would not be possible for all T_s values simply because, in some cases, an eddy measured by the sonic anemometer might ~~be~~ never be sampled by the χ_{H2O} sampling orifice, and vice versa (see Section 5.2~~6~~). Realistically, T_s may be matched with χ_{H2O} overall with the most likelihood as many pairs as possible for a period (e.g., an averaging interval).

The match is eventually to lag either T_s or χ_{H2O}, relatively, in the synchronization matrix (28). The lag can be counted as an integer number (l_s, subscript *s* indicates the spatial separation causing lag) in measurement intervals where l_s is positive if an eddy flowed through the T_s measurement volume earlier, negative if later, or zero if through the χ_{H2O} sampling orifice at the same time. This number is estimated through the covariance maximization (Irwin, 1979; Moncrieff et al., 1997; Ibrom~~e~~ et al., 2007; Rebmann et al., 2012). According to l_s over an averaging interval, the data columns of the gas analyzer over an averaging interval in the synchronization matrix (28) can be moved together up l_s rows as positive, down l_s rows as negative, or nowhere as zero to form a matched matrix:

$$\begin{bmatrix} \cdots\cdots\cdots\cdots \\ u(t_i) \;\; v(t_i) \;\; w(t_i) \;\; T_s(t_i) \;\; d_s(t_i) \;\; \chi_{H_2O}(t_{i+l_s}) \;\; d_g(t_{i+l_s}) \;\; s(t_{i+l_s}) \\ \cdots\cdots\cdots\cdots \end{bmatrix} \tag{29}$$

For details to find l_s, see EasyFlux-DL-CR6CP on https://www.campbellsci.com. In the matched matrix, over an averaging interval, a pair of T_s and χ_{H2O} in the same row can be assumed to be matched as if measured and sampled from the same eddy.

Using Eq. (23), the air temperature now can be computed using:

$$T_{l_s i} = T_s(t_i)\frac{\left[1+\varepsilon\chi_{H_2O}(t_{i+l_s})\right]\left[1+\varepsilon\gamma_v\chi_{H_2O}(t_{i+l_s})\right]}{\left[1+\chi_{H_2O}(t_{i+l_s})\right]\left[1+\varepsilon\gamma_p\chi_{H_2O}(t_{i+l_s})\right]} \tag{30}$$

where subscript l_s for T indicates that spatially lagged χ_{H2O} is used for computation of T. In verification for the accuracy of equation-computed T and in assessments on its expected advantages of high-frequency signal insensitive to solar contamination in measurements, $T_{l_s i}$ could minimize the uncertainties due to the spatial separation in measurements of T_s and χ_{H2O} between the T_s measurement volume and the χ_{H2O} sampling orifice (Fig. 1).

6 Results

6.1 ~~8~~ Verification ~~f~~o~~f~~ the accuracy of equation-computed T

The accuracy of equation-computed T was theoretically specified by Eqs. (25) to (27) and was estimated in Fig. 2c. This accuracy specifies the range of equation-computed minus true T (i.e., ΔT). However, the true T was not available in the field but, as usual, precision measurements could be considered as a benchmark to represent the true T. In this study, T measured by the RTD inside a fan-aspirated radiation shield (T_{RTD}) was the benchmark to compute ΔT (i.e., equation-computed T minus T_{RTD}). If almost all ΔT values fall within the accuracy-specified range over a measurement domain of T_c and χ_{H2O}, the accuracy is correctly defined and the equation-computed T is accurate as specified.

To verify the accuracy over the domain as large as possible, ΔT values in the coldest (January) and hottest (July) months were used as shown in Fig. 4 (-21 ºC < T_c < 35.5 ºC and χ_{H2O} up to 20.78 mmolH_2O mol^{-1} in a 30-minute mean over the two months). Out of 2,976 ΔT values from both months, 44 values fell out of specified-accuracy range, but near the range line within 0.30 K. The ΔT values were 0.549 ± 0.281 K in January and 0.436 ± 0.290 K in July. Although these values were almost all positively away from the zero-line due to either overestimation for T_s by the sonic anemometer within ± 1.00 K accuracy or underestimation for T_{RTD} by the RTD within ± 0.20 K accuracy, the ranges are significantly narrower than the specified accuracy range of equation-computed T (Figs. 2c and 4). ~~Therefore, the equation-computed T is accurate as specified and even much better.~~

It is common for sonic anemometers to have a systematic error in T_s to be ±0.5 ºC or a little greater, which is the reason that the T_s accuracy is specified by Larry Jacobsen (anemometer authority) to be ±1.0 ºC for the updated CSAT3A. The fixed deviation in measurements of sonic path lengths is asserted as a source for bias of T_s (Zhou et al., 2018). This bias brings an error to equation-computed T. If the T equation were not exact as Eqs. (4) and (5), there would be an additional equation error. In our study effort, this bias from fixed deviation possibly is around 0.5 ºC. With this bias, the equation-computed T is still accurate as specified by Eqs. (25) to (27) and even better.

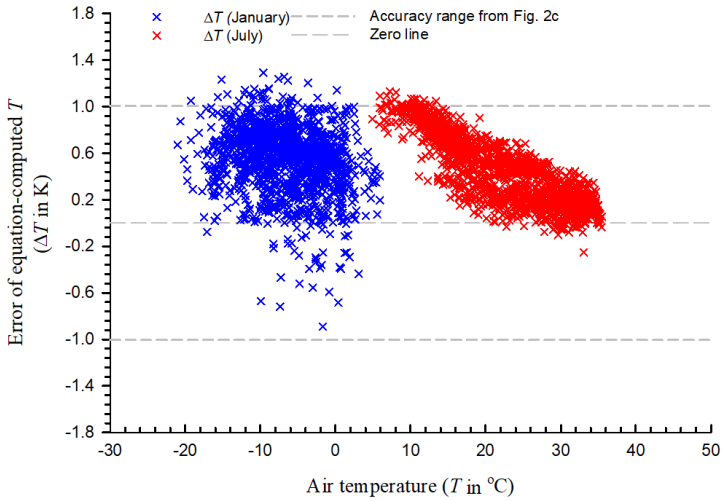

Figure 4: The error of equation-computed *T* in coldest (January) and hottest (July) months, 2019 in Logan, UT, US. *ΔT* is equation-computed minus RTD-measured *T* where RTD is a precision platinum resistance temperature detector inside a fan-aspirated radiation shield. *ΔT*: 0.549 ± 0.281 K in January and 0.436 ± 0.290 K in July. See Fig. 2c for the accuracy range.

6.2 ~~9~~ Assessments of the advantages of equation-computed *T*

As previously discussed, the data stream of equation-computed *T* consists of high-frequency signals insensitive to solar contamination in measurements. Its frequency response can be assessed against known high-frequency signals of T_s, and the insensitivity can be assessed by analyzing the equation-computed, RTD~~T~~-measured, and sensor-measured T_s where the sensor is HMP155A inside a wind-aspirated radiation shield.

6.2.1 ~~9.1~~ Frequency response

The matched matrix (29) and Eq. (30) were used to compute $T_{i,i}$ (i.e., equation-computed *T*). Paired power spectra of equation-computed *T* and T_s are compared in Fig. 5 for three individual two-hour periods of atmospheric stratifications, including unstable (z/L = -0.313 ~ -2.999 where *z* is a dynamic height of measurement minus displacement height and *L* is the Monin-Obukhov length), near- neutral (z/L = -0.029 ~ +0.003), and stable (z/L = +0.166 ~ +0.600) ~~atmospheric stratifications~~. Slower response of equation-computed *T* than T_s at higher frequency (e.g. > 5 Hz) was expected because equation-computed *T* is derived from two variables (T_s and χ_{H2O}) measured in a spatial separation, which attenuates the frequency response of correlation of two measured variables (Laubach and McNaughton, 1998), and χ_{H2O} from a CPEC system has slower response than T_s in frequency (Ibrom et al., 2007). However, the expected slower response was not found in this study. In unstable and stable atmospheric stratifications (~~panels a and c of~~ Fig. 5a and 5c), each pair of power spectra almost overlap. Although they do not overlap in the near-neutral atmospheric stratification (Fig. 5b), the pair follow the same trend slightly above or below one another. In the higher frequency band of 1 to 10 Hz in ~~panels a and b of~~ Figs. 5a and 5b, equation-computed *T* has a little more power than T_s. The three pairs of

power spectra in Fig. 5 indicate that equation-computed T has a frequency reponse equialvelent to T_s up to 10 Hz, with a at 20-Hz measurent rate considered to beas a high frequency. The equivalent response might be accounted for by a dominant role of T_s in the magnitude of equation-computed T.

500

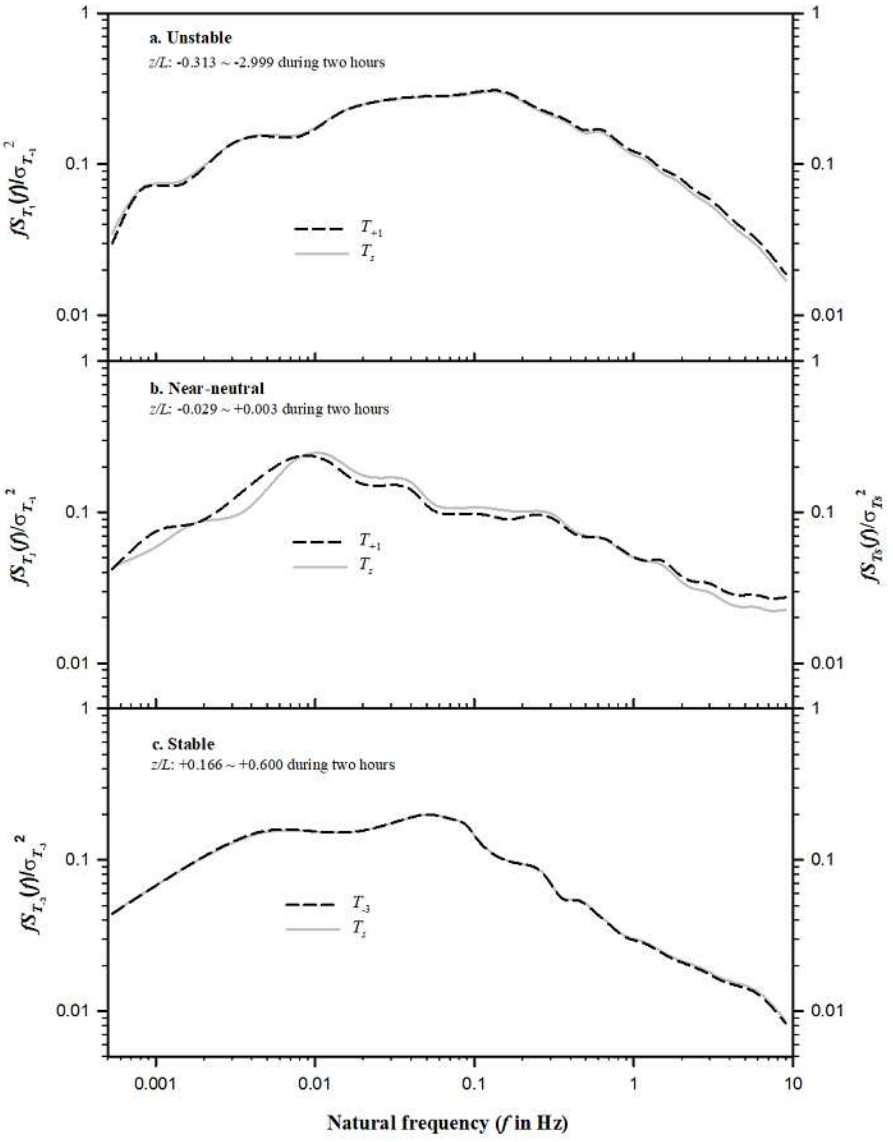

Figure 5: Paired comparisons of power spectra for equation-computed air temperature (*T*) and sonic temperature (T_s) at each of three atmospheric stratifications: unstable (a), near-neutral (b), and stable (c). T_1 and T_{-3} are equation-computed *T* from T_s and the H_2O mixing ratio of air sampled by the CPEC system through its sampling orifice in 1 lag (50 ms behind ~~(1 lag)~~ and in -3 lags (150 ms ahead ~~(-3 lags)~~ of T_s measurement; *z* is the dynamic height of measurement minus displacement height, *L* is Monin-Obukhov length, $S_{T_s}(f)$, $S_{T_1}(f)$ and $S_{T_{-3}}(f)$ are the power spctra of T_s, T_1, and T_{-3} at *f*; and $\sigma^2_{T_s}$, $\sigma^2_{T_1}$ and $\sigma^2_{T_{-3}}$ represent ~~are~~ the variance of T_s, T_1, and T_{-3}.

6.2.2 ~~9.2~~ Insensitivity to solar contamination in measurements

The data of equation-computed, sensor-measured, and RTD~~T~~-measured T in July, during which incoming solar radiation (R_s) in the site was strongest in a yearly cycle, are used to assess the insensitivity of equation-computed T. From the data, ΔT is considered as an error of equation-computed T. The error of sensor-measured T can be defined as sensor-measured minus RTD~~T~~-measured T, denoted by ΔT_m. From Fig. 6, ΔT (0.690 ± 0.191 K) is > ΔT_m (0.037 ± 0.199 K) when R_s < 50 W m^{-2} at lower radiation. However, ΔT (0.234 ± 0.172 K) is < ΔT_m (0.438 ± 0.207 K) when R_s > 50 W m^{-2} at higher radiation. This difference between ΔT and ΔT_m shows a different effect of R_s on equation-computed and sensor-measured T.

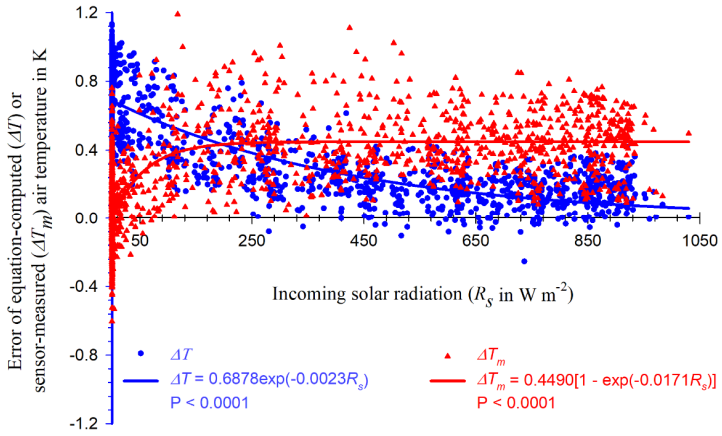

Figure 6: Errors in equation-computed and sensor-measured air temperature (*T*) with incoming solar radiation. ΔT is equation-computed minus RTD-measured ~~air temperature~~ *T*, where the RTD is a precision platinum resistance temperature detector inside a fan-aspirated radiation shield. ΔT_m is sensor-measured minus RTD-measured *T*, ~~air temperature~~ where the sensor is a HMP155A air temperature and humidity probe inside a wind-aspirated radiation shield.

As shown ~~from~~in Fig. 6, ΔT_m increases sharply with increasing R_s for R_s < 250 W m^{-2}, beyond which it asymptotically approaches 0.40 K. In the range of lower R_s, atmospheric stratification was likely stable (Kaimal and Finnigan, 1994) under which the heat exchange by wind was ineffective between the wind-aspirated radiation shield and boundary-layer flows. In this case, sensor-measured T was expected to increase with R_s increase (Lin et al., 2001; Blonquist and Bugbee, 2018). Along with R_s increase, the atmospheric boundary-layer develops from stable to neutral or unstable conditions (Kaimal and Finnigan, 1994). During the stability change, the exchange becomes increasingly more effective, offsetting the further heating from R_s increase on the wind-aspirated radiation shield as indicated by the red asymptote portion in Fig. 6. Compared to the ΔT_m mean (0.037 K) while R_s < 50 W m^{-2}, the magnitude of the asymptote above the mean is the over-estimation of sensor-measured T due to solar contamination.

However, ΔT decreases asymptotically from about 0.70 K toward zero with the increase in R_s from 50 to 250 W m^{-2} and beyond, with a more gradual rate of change than ΔT_m at the lower radiation range. Lower R_s (e.g., < 250 W m^{-2}) concurrently occurs with lower T_c, higher RH, and/or unfavorable weather to T_s measurements. Under lower T_c (e.g., below 20 ºC of CSAT3A manufacture conditions), the sonic path lengths of CSAT3A (Fig. 1) must become, due to thermo-contraction of sonic anemometer structure, shorter than those at 20 ºC. As a result, the sonic anemometer could over-estimate the speed of sound

(Zhou et al., 2018) and hence T_s for equation-computed T, resulting in greater ΔT with lower R_s. Under higher RH conditions, dew may form on the sensing surface of six CSAT3A ~~six~~ sonic transducers (Fig. 1). The dew, along with unfavorable weather, could contaminate the T_s measurements, resulting in greater ΔT in magnitude. Higher R_s (e.g., > 250 W m^{-2}) concurrently occurs with weather favorable to T_s measurements, which is the reason that ΔT slightly decreases rather than increases with R_s when R_s > 250 W m^{-2}.

Again from Fig. 6, the data pattern of $\Delta T > \Delta T_m$ in the lower R_s range and $\Delta T < \Delta T_m$ in the higher R_s range shows that equation-computed T is not as sensitive to R_s as sensor-measured T. The decreasing trend of ΔT with R_s increase shows the insensitivity of equation-computed T to R_s. Although the purpose of this study is not particularly to eliminate solar radiation contamination, equation-computed T is indeed less contaminated by solar radiation as shown in Fig. 6.

7 ~~10~~ Discussion

7.1 ~~10.1~~ Actual accuracy

The range of ΔT curves for each RH level in Fig. 2 is the maximum at that level because the data were evaluated using the maximized measurement uncertainties from all sources. Accordingly, in field applications under weather favorable to T_s measurements, the range of actual accuracy in equation-computed T can be reasonably inferred to be narrower. In our study case as shown in Figs. 4 and 6, the variability of ΔT was narrower than the accuracy range as specified in Fig. 2. In other words, ~~T~~the actual accuracy is better.

However, under weather conditions unfavorable to T_s measurements such as dew, rain, snow, or dust storm, the accuracy of T_s measurements cannot be easily evaluated. T_s measurements also possibly have a systematic error due to the fixed deviation in the measurements of sonic path lengths for sonic anemometers although the error should be within the accuracy specified in Fig. 2. A χ_{H2O} measurement also can be erroneous if the gas analyzer is not periodically zeroed and spanned for its measurement environment. Therefore, if T_s is measured under unfavorable weather conditions~~,~~ and the sonic anemometer produces a systematic T_s error, and if the gas analyzer is not zeroed and spanned as instructed in its manual,~~;~~ then the accuracy of equation-computed T would be unpredictable. Normally, the actual accuracy is better than that ~~e one~~ specified in Fig. 2. Additionally, with the improvement in measurement accuracies of sonic anemometers ~~[~~(e.g., ~~W~~weather-condition-regulated, heated 3-D sonic anemometers, Mahan et al., ~~(~~2021)] and gas analyzers, this accuracy of equation-computed T would ~~be~~ gradually becom~~e~~ing better ~~and better~~.

For this study, filtering out the T_s data in the periods of unfavorable weather could narrow the error range of equation-computed T. The unfavorable weather was suspected to contribute to the stated error. However, although filtering out unfavorable weather cases could create a lower error estimate, most field experiments include periods when weather increases a T_s error, so including a weather contribution to error would prevent overstating instrument accuracy under typical (unfiltered) applications. Therefore, both T_s and χ_{H2O} data in this study were not programmatically or manually filtered based on weather.

7.2 ~~10.2~~ Spatial separation of T_s and χ_{H2O} in measurements

In this study, T was successfully computed from ~~the~~ T_s and χ_{H2O} as a high-frequency signal (Fig. 5) with expected accuracy as tested in Figs. 2, 4 and 6, where both were measured separately from two sensors in a spatial separation. Some open-path eddy-covariance (OPEC) flux systems (e.g., CSAT3A+EC150 and CSAT3B+LI7500) measure T_s and ρ_w also from two sensors in a spatial separation. To OPEC systems, although the air temperature equation (Eq. 23) is not applicable, the algorithms developed

in Section 5.3~~7~~ to temporally synchronize and spatially match T_s with χ_{H2O} for computation of T are applicable for computation of T from T_s and ρ_w along with P in such OPEC systems (Swiatek, 2018).

In Section 5.3~~7~~, programing and computing are needed to pair T_s measured to χ_{H2O} sampled at the same time into synchronization matrix (28) as the first step and from the same eddy into matched matrix (29) as the second step. The second requires complicated programing and much computing. To test the necessity of this step in specific cases, using Eq. (30), T_{0i} was computed from a row of the synchronization matrix and $T_{l_s i}$ was computed from this matrix by lagging χ_{H2O} columns up l_s rows if $l_s > 0$ and down $|l_s|$ rows if $l_s < 0$ where l_s is -5, ……, -1, +1, ……, +5. From the data of this study, individual $T_{l_s i}$ values were different for different subscript l_s, but their means for subscript i over an averaging interval (T_{l_s}) are the same to at least the fourth digit after the decimal place. Further, the power spectum of T_{0i} time series was compared to those of $T_{l_s i}$ time series, where $i \neq 0$. Any pair of power spectra from the same period overlap exactly (Figures omitted). Therfore, the second step of lag maximization to match T_s measured to χ_{H2O} sampled from the same eddy is not needed if only hourly mean and power spectrum of equation-computed T are of interest to computations, for both CPEC and OPEC systems.

7.3 ~~10.3~~ Applications

The air temperature equation (23) is derived from first principles without any assumption and approximation. It is an exact equation from which T can be computed in CPEC systems as a high-frequency signal insensitive to solar radiation. These merits in additional to its consistent representation of spatial measurement and temporal synchronization scales with other thermodynamic variables for boundary-layer turbulent flows will be more needed for advanced applications. Popularly used in the world, EasyFlux series is one of the two field eddy-covariance flux software packages, in which the other inscluded is EddyPro (LI-COR Biosciences, 2015). Currently, it has used equation-computed T for ρ_d in Eq. (1), sensible heat flux (H), and RH as a high-frequency signal in CPEC systems (Campbell Scientific Inc. 2018a).

~~The air temperature equation (Eq. 23) is derived from first principles without any assumption and approximation. It is an exact equation from which T can be computed in a CPEC system as a high-frequency signal insensitive to solar radiation. Therefore, this equation is applicable to calculations of ρ_d in Eq. (1), sensible heat flux from T_s in a possible way different from Schotanus et al. (1983) or van Dijk (2002), and RH as a highfrequency signal in a CPEC system.~~

7~~10~~.3.1 Dry air density

As a high-frequency signal insensitive to solar radiation, equation-computed T is more applicable than sensor-measured T for calculations of $\overline{\rho}_d$ and $\overline{\rho_d w}$ for more applications (Gu et al., 2012; Foken et al., 2012). In practice, equation-computed T may be used for $\overline{\rho}_d$ and $\overline{\rho_d w}$ under normal weather conditions while the sonic anemometer and gas analyzer are normally running, which can be judged by their diagnosis codes (Campbell Scientific Inc., 2018a). Under a weather condition unfavorable to T_s measurements due to dew, rain, snow, and ice conditions,~~;~~ equation-computed T from weather-condition-regulated, heated 3-D sonic anemometers (Mahan et al., 2021) and CPEC infrared ~~gas~~ analyzer could be an alternative.

Currently, in CO_2, H_2O and trace gas flux measurements, mean ρ_d for flux calculations is estimated from T and RH along with P. T and RH are measured mostly by a slow-response T-RH probe without fan-aspiration (e.g., HMP155A. Zhu et al.,

2021). As shown in Fig. 6, equation-computed T is better than probe-measured T. The air moisture measured by an infrared analyzer in CPEC systems must be more accurate [Eq. (27) and Fig. 2b] than probe-measured air moisture. The better equation-computed T along with more accurate air moisture has no reason not to improve the estimation for mean ρ_d.

7~~10~~.3.2 Sensible heat flux estimated from an CPEC system

Currently, sensible heat flux (H) is derived from $\overline{T_s'w'}$ with a humidity correction (van Dijk, 2002). The correction equations were derived by Schotanus et al. (1983) and van Dijk (2002) in two ways, but both from Eq. (4) derived with approximation (see Appendix A). Using the exact equation from this study, theoretically, H can be more accurately estimated directly from $\overline{T'w'}$, where T is the equation-computed air temperature, although studies and tests for this potential application are needed. Without our exact T equation, in any flux software, either Eq. (4) or (5) must to be used for sensible heat flux computation. Both equations are approximate (see Appendices A and B). Compared to either, our exact equation must be an improvement on the mathematical representation of sensible heat flux. If the equation for sensible heat flux is approximate, then even a perfect measurement gives only an approximate value for the flux.

7~~10~~.3.3 RH as a high frequency signal

Conventionally, RH is measured using a temperature and humidity probe, which is unable to track the high frequency fluctuations of RH. In a CPEC system, equation-computed T, gas-analyzer-measured χ_{H_2O}, and transducer-measured P are able to catch the fluctuations in these variables at high frequency, from which RH can be computed (Sonntag, 1990; also see Appendix C). This method should provide high frequency RH, although verification is needed. Currently, the applications of high frequency properties in this RH are unknown in a CPEC system. Regardless, equation-computed T provides a ~~a~~ potential opportunity to acquire the high frequency RH for its application in the future.

8 ~~11~~ Concluding remarks

In a CPEC flux system, the air temperatrure (T) of boundary-layer flows through the space of sonic anemometer measurement and infrared analyzer sampling (Fig. 1) is desired for high frequency (e.g., 10 Hz) with consistent representation of spatial and temporal scales for moist turbulence thermodynamics characterized by three-dimensional wind from the sonic anemometer and H_2O/CO_2 and atmospheric pressure from the gas analyzer measurements. High-frequency T in the space can be measured using fine~~-~~wire thermocouples, but this kind of thermocouple~~s~~ for such an application is not durable under adverse climate conditions, being easily contaminated by solar radiation (Campbell, 1969). Nevertheless, the measurements of sonic temperature (T_s) and H_2O inside a CPEC system are high~~-~~frequency signals. Therefore, high-frequency T can be reasonably expected when computed from T_s and H_2O-related variables. For this expectation, two equations [i.e., Eqs. (4) and (5)] are currently available. In both equations, converting H_2O-related variables into H_2O mixing ratio analytically reveals the difference between the two equations. This difference in CPEC systems reaches ±0.18 K, bringing an uncertainty into the accuracy of T from either equation and raising a question of which equation is better. To clarify the uncertainty and answer this question, the air temperature equations in terms of T_s and H_2O-related variables are thoroughly reviewed (Sections 2 and 3~~,~~ Appendices A and B). The two currently used equations [i.e., Eqs. (4) and (5)] were developed and completed with approximations (Appendices A and B). Because of the approximations, neither of their accuracies was ~~were~~ evaluated, nor was the question answered.

Using the first principles equations, the air temperature equation in terms of T_s and χ_{H_2O} (H_2O mixing ratio) is derived without any assumption and approximation ~~([~~Eq. (23)~~]~~; therefore, the equation derived in this study does not, itself, have any error and, as such, the accuracy in equation-computed T depends solely on the measurement accuracies of T_s and χ_{H_2O}. Based on the specifications for T_s and χ_{H_2O} in the CPEC300 series, the accuracy of equation-computed T over the T_s and χ_{H_2O} measurement ranges can be specified within ±1.01K (Fig. 2). This accuracy range ~~uncertainty~~ is propagated mainly (±1.00 K) from the uncertainty in T_s measurements (Fig. 2a) and little (±0.02 K) from the uncertainty in χ_{H_2O} measurements (Fig. 2b).

Under normal sensor and weather conditions, the specified accuracy is verified based on field data as valid and actual accuracy is better (Figs. 4 and 6). Field data demonstrate~~d~~ that equation-computed T under unstable, near-neutral, and stable atmospheric stratifications all have frequency responses equivalvelent to high-frequency T_s up to 10 Hz at a 20-Hz measurement rate (Fig. 5), being insensitive to solar contamination in measurements (Fig. 6).

The current applications of equation-computed T in a CPEC system are to calculate dry air density (ρ_d) for the estimations of CO_2 flux ($\overline{\rho}_d \overline{\chi'_{CO_2} w'}$, where χ_{CO_2} is CO_2 mixing ratio, w is vertical velocity of air, and prime indicates the fluctuation of variable away from its mean as indicated by overbar. e.g., $w' = w - \overline{w}$), H_2O flux ($\overline{\rho}_d \overline{\chi'_{H_2O} w'}$), and other fluxes. Combined with measurements of χ_{H_2O}, 3-D wind speeds, and P, the equation-computed T can ~~be~~ potentially be applied to the estimation of $\overline{\rho}_d$ and $\overline{\rho_d w}$ (Gu et al., 2012; Foken et al., 2012), to the computation of high-frequency RH (Sonntag, 1990), and to the derivation of sensible heat flux (H) avoiding the humidity correction as needed for H indirectly from T_s (Schotanus et al., 1983; van Dijk, 2002).

In a CPEC flux system, although T_s and χ_{H_2O} are measured using two spatially separated sensors of sonic anemometer and infrared ~~gas~~ analyzer, T was successfully computed from both measured variables as a high-frequency signal (Fig. 5) with an expected accuracy (Figs. 2 and 4). Some open-path eddy-covariance (OPEC) flux systems measure T_s and water vapor density (ρ_w) also from two sensors in a similar way. The algorithms developed in Section 5.3~~7~~ to temporally synchronize and spatially match T_s with χ_{H_2O} for computation of T are applicable to such an OPEC system to compute T from T_s and ρ_w along with P. This T would be a better option than sensor-measured T in the system for the correction of spectroscopic effect in measuring CO_2 fluctuations at high frequencies (Helbig et al., 2016; Wang et al., 2016). With the improvements on measurement technologies for T_s and χ_{H_2O}, particularly for T_s, the T from our developed equation will become increasingly more accurate. Having its accuracy combined with its high frequency, this T with consistent representation of all other thermodynamic variables for moist air at the spatial and temporal scales in CPEC measurements has its advanced merits in boundary-layer meteorology and applied meteorology.

Field Code Changed

Appendices

Appendix A. Derivation of e~~E~~quation (4)

The sonic temperature (T_s) reported by a three-dimensional sonic anemometer ~~thermometry~~ is internally calculated from its measurements of the speed of sound in moist air (c) after the crosswind correction (Zhou et al., 2018), using

$$T_s = \frac{c^2}{\gamma_d R_d}, \quad \text{(a1)}$$

where subscript d indicates dry air, γ_d is the specific heat ratio of dry air between constant pressure and constant volume, and R_d is gas constant for dry air (Campbell Scientific Inc., 2018b). The speed of sound in the atmospheric boundary-layer as in a homogeneous gaseous medium is well defined in acoustics (Barrett and Suomi, 1949), given by:

$$c^2 = \gamma \frac{P}{\rho}, \quad \text{(a2)}$$

where γ is the counterpart of γ_d for moist air, P is atmospheric pressure, and ρ is moist air density. These variables are related to air temperature and air specific humidity (q, i.e., the mass ratio of water vapor to moist air).

1. Moist air density (ρ)

Moist air density is the sum of dry air and water vapor densities. Based on the ideal gas law (Wallace and Hobbs, 2006), dry air density (ρ_d) is given by:

$$\rho_d = \frac{P - e}{R_d T}, \quad \text{(a3)}$$

where e is water vapor pressure, and the water vapor density (ρ_w) is given by:

$$\rho_w = \frac{e}{R_v T}, \quad \text{(a4)}$$

where R_v is the gas constant for water vapor. Therefore, moist air density in Eq. (a2) can be expressed as:

$$\rho = \frac{P - e}{R_d T} + \frac{e}{R_v T}. \quad \text{(a5)}$$

Because of $R_d/R_v = \varepsilon$ (i.e., 0.622, the molar mass ratio between water vapor and dry air), this equation can be rearranged as:

$$\rho = \frac{P}{R_d T}\left[1 - (1 - \varepsilon)\frac{e}{P}\right]. \quad \text{(a6)}$$

Using Eqs. (a4) and (a6), the air specific humidity can be expressed as:

$$q \equiv \frac{\rho_w}{\rho} = \frac{\varepsilon e}{P - (1 - \varepsilon)e}. \quad \text{(a7)}$$

Because of $P >> (1 - \varepsilon)e$, q can be approximated as:

$$q \approx \varepsilon \frac{e}{P}. \quad \text{(a8)}$$

Substituting this relation into Eq. (a6) generates:

$$\rho = \frac{P}{R_d T}\left(1 - \frac{1 - \varepsilon}{\varepsilon} q\right). \quad \text{(a9)}$$

2. Specific heat ratio of moist air (γ)

The specific heat ratio of moist air is determined by two moist air properties: 1) the specific heat at constant pressure (C_p) and 2) specific heat at constant volume (C_v). C_p varies with the air moisture content between the specific heat of dry air at constant pressure (C_{pd}) and the specific heat of water vapor at constant pressure (C_{pw}). It must be the average of C_{pd} and C_{pw} that is ~~are~~ arithmetically weighted by dry air mass and water vapor mass, respectively, given by (Stull, 1988):

$$C_p = \frac{C_{pd}\rho_d + C_{pw}\rho_w}{\rho}. \quad \text{(a10)}$$

C_v can be similarly determined:

$$C_v = \frac{C_{vd}\rho_d + C_{vw}\rho_w}{\rho}, \quad \text{(a11)}$$

where C_{vd} is the specific heat of dry air at constant volume and C_{vw} is the specific heat of water vapor at constant volume. Denoting C_{pd}/C_{vd} as γ_d, Eqs. (a10) and (a11) are used to express γ as:

$$\gamma = \frac{C_p}{C_v} = \gamma_d \frac{(1-q) + qC_{pw}/C_{pd}}{(1-q) + qC_{vw}/C_{vd}}. \quad \text{(a12)}$$

3. Relate sonic temperature to air temperature

Substituting Eqs. (a9) and (a12) into Eq. (a2) leads to:

$$c^2 = \gamma_d R_d T \frac{(1-q) + qC_{pw}/C_{pd}}{\left[(1-q) + qC_{vw}/C_{vd}\right]\left(1 - \frac{1-\varepsilon}{\varepsilon}q\right)}. \quad \text{(a13)}$$

Using this equation to replace c^2 in Eq. (a1), T_s is expressed as:

$$T_s = T \frac{(1-q) + qC_{pw}/C_{pd}}{\left[(1-q) + qC_{vw}/C_{vd}\right]\left(1 - \frac{1-\varepsilon}{\varepsilon}q\right)}. \quad \text{(a14)}$$

Given C_{pw} = 1,952, C_{pd} = 1,004, C_{vw} =1,463, and C_{vd} = 717 J K^{-1} kg^{-1} (Wallace and Hobbs, 2006); this equation becomes:

$$T_s = T(1 + 0.944223q)\left(\frac{1}{1 + 1.040446q}\right)\left(\frac{1}{1 - 0.607717q}\right). \quad \text{(a15)}$$

Expression of the last two parenthesized terms in the right side of this equation separately as Taylor series of q (Burden and Faires, 1993) by dropping, due to $q << 1$, the second or higher terms related to q leads to:

$$T_s \approx T(1 + 0.944223q)(1 - 1.040446q)(1 + 0.607717q). \quad \text{(a16)}$$

In the right side of this equation, the three parenthesized terms can be expanded into a polynomial of q at the third order. Also due to $q << 1$ in this polynomial, the terms of q at the second or third order can be dropped. Further arithmetical manipulations result in:

$$T_s \approx T(1 + 0.51q). \quad \text{(a17)}$$

This is Eq. (4) in a different form. In its derivations from Eqs. (a1) and (a2), three approximation procedures were used from Eqs. (a7) to (a8), (a15) to (a16), and (a16) to (a17). The three approximations must bring unspecified errors into the derived equation.

Appendix B. Derivation of equation (5)

Equation (5) was sourced from Ishii (1932) in which the speed of sound in moist air (c) was expressed in his Eq. (1) as:

$$c^2 = \gamma\left(\frac{P}{\rho}\right)\left(\frac{\alpha}{\beta}\right), \quad \text{(b1)}$$

where all variables in this equation are for moist air, γ is the specific heat ratio of moist air between constant pressure and constant volume, P is moist air pressure, ρ is moist air density, α is moist air expansion coefficient, and β is moist air pressure coefficient. Accordingly, the speed of sound in dry air (c_d) is given by:

$$c_d^2 = \gamma_d \left(\frac{P_d}{\rho_d}\right)\left(\frac{\alpha_d}{\beta_d}\right), \tag{b2}$$

where subscript d indicates dry air in which γ_d, P_d, ρ_d, α_d, and β_d are the counterparts of γ, P, ρ, α, and β in moist air. Equations (b1) and (b2) can be combined as:

$$c^2 = c_d^2\left(\frac{\gamma}{\gamma_d}\right)\left(\frac{P\rho_d}{P_d\rho}\right)\left(\frac{\alpha\beta_d}{\alpha_d\beta}\right). \tag{b3}$$

Experimentally by Ishii (1932), each term inside the three pairs of parentheses in this equation was linearly related to the ratio of water vapor pressure (e) to dry air pressure (P_d). The relationship into Eq. (b3) leads to:

$$c^2 = c_d^2\left(1+0.00163\frac{e}{P_d}\right)\left(1-0.378\frac{e}{P_d}\right)^{-1}\left(1-0.0613\frac{e}{P_d}\right). \tag{b4}$$

The three parenthesized terms in this equation are sequentially corresponding to the three parenthesized terms in Eq. (b3). Dividing $\gamma_d R_d$, where R_d is gas constant for dry air, over both sides of Eq. (b4) and reference Eq. (11), sonic temperature (T_s) is expressed in terms of air temperature (T), e, and P_d as:

$$T_s = T\left(1+0.00163\frac{e}{P_d}\right)\left(1-0.378\frac{e}{P_d}\right)^{-1}\left(1-0.0613\frac{e}{P_d}\right). \tag{b5}$$

Using the relationship of $P_d = P - e$, this equation can be manipulated as:

$$\begin{aligned} T_s &= T\left(\frac{P-0.9984e}{P-e}\right)\left(\frac{P-1.3780e}{P-e}\right)^{-1}\left(\frac{P-1.0613e}{P-e}\right) \\ &= T\left(\frac{P-0.9984e}{P-e}\right)\left(\frac{P-1.0613e}{P-1.3780e}\right) \\ &= T\frac{1-2.0597e/P+1.0596(e/P)^2}{1-2.3780e/P+1.3780(e/P)^2} \end{aligned} \tag{b6}$$

Dropping the second order terms due to $e/P << 1$ in boundary-layer flows, this equation becomes:

$$T_s \approx T\left(1-2.0597\frac{e}{P}\right)\left(1-2.3780\frac{e}{P}\right)^{-1}. \tag{b7}$$

Expanding the second parenthesized term into Taylor series and, also due to $e/P << 1$, dropping the terms related to e/P at an order of second or higher, this equation becomes:

$$T_s \approx T\left(1-2.0597\frac{e}{P}\right)\left(1+2.3780\frac{e}{P}\right). \tag{b8}$$

Further expanding the two parenthesized terms in the right side of this equation and dropping the second order term of e/P lead to:

$$T_s \approx T\left(1+0.32\frac{e}{P}\right). \quad \text{(b9)}$$

This is Eq. (5) in a different form. From the experimental source of Eq. (b4), it was derived using three approximations from Eq. (b4) to (b7), (b7) to (b8), and (b8) to (b9). The approximations, **and therefore** combined uncertainty in *T* ~~therefore~~, bring unspecified errors into Eq. (5) [i.e., Eq. (b9)] as an equation error.

Appendix C. Water vapor mixing ratio and sonic temperature from relative humidity, air temperature, and atmospheric pressure

For a given air temperature (T in °C) and atmospheric pressure (P in kPa), air has a limited capacity to hold water vapor (Wallace and Hobbs, 2006). This limited capacity is described in terms of saturation water vapor pressure (e_s in kPa) for moist air, given through the Clausius-Clapeyron equation (Sonntag, 1990):

$$e_s(T,P)=\begin{cases}0.6112\exp\left(\dfrac{17.62T}{T+243.12}\right)f(P) & T\geq 0\\ 0.6112\exp\left(\dfrac{22.46T}{T+272.62}\right)f(P) & T<0\end{cases} \quad \text{(c1)}$$

~~W~~where $f(P)$ is an enhancement factor for moist air, being a function of atmospheric pressure: $f(P)=1.0016+3.15\times10^{-5}P-0.0074P^{-1}$. At relative humidity (RH in %), the water vapor pressure [$e_{\mathrm{RH}}(T,P)$] is:

$$e_{\mathbf{RH}}(T,P)=\frac{\mathrm{RH}}{100}e_s(T,P). \quad \text{(c2)}$$

Given the mole numbers of H_2O (n_{RH}) and dry air (n_d) at RH, the H_2O molar ~~water vapor~~ mixing ratio at RH ($\chi^{\mathrm{RH}}_{H_2O}$):

$$\chi^{\mathrm{RH}}_{H_2O}\equiv\frac{n_{\mathbf{RH}}}{n_d}=\frac{n_{\mathbf{RH}}R^*(T+273.15)}{n_dR^*(T+273.15)}=\frac{e_{\mathrm{RH}}(T,P)}{P_d} \quad \text{(c3)}$$

where R^* is the universal gas constant and P_d is dry air pressure. Using this equation and the relation:

$$P=P_d+e_{\mathrm{RH}}(T,P), \quad \text{(c4)}$$

$\chi^{\mathrm{RH}}_{H_2O}$ can be expressed as:

$$\chi^{\mathrm{RH}}_{H_2O}=\frac{e_{\mathrm{RH}}(T,P)}{P-e_{\mathrm{RH}}(T,P)} \quad \text{(c5)}$$

Using Eq. (23), this $\chi^{\mathrm{RH}}_{H_2O}$ along with T_c can be used to calculate sonic temperature (T_s) at RH, given by:

$$T_s\left(T,\chi^{\mathrm{RH}}_{H_2O}\right)=(T+273.15)\frac{\left(1+\chi^{\mathbf{RH}}_{H_2O}\right)\left(1+\varepsilon\gamma_p\chi^{\mathbf{RH}}_{H_2O}\right)}{\left(1+\varepsilon\chi^{\mathbf{RH}}_{H_2O}\right)\left(1+\varepsilon\gamma_v\chi^{\mathbf{RH}}_{H_2O}\right)} \quad \text{(c6)}$$

where $\varepsilon=0.622$ (Eq. 17), $\gamma_v=2.04045$, and $\gamma_p=1.94422$ (Eq. 23). Through Eqs. (c1) and (c2), Eqs. (c5) and (c6)

express $\chi_{H_2O}^{RH}$ and $T_s(T,\chi_{H_2O}^{RH})$, respectively, in terms of *T*, RH, and *P*. $\chi_{H_2O}^{RH}$ and $T_s(T,\chi_{H_2O}^{RH})$ can be used to replace χ_{H_2O} (H_2O molar ~~water vapor~~ mixing ratio) and T_s in Eq. (25). After replacements, Eq. (25) can be used to evaluate the uncertainty, due to T_s and χ_{H_2O} measurement accuracy uncertainties, in air temperature computed from Eq. (23) for different *RH* values over a *T* range.

Author Contribution~~s~~.

JZ led this work; XinZ, TG, and XiaoZ derived equations, analyzed data, and drafted the manuscript; ET substantially structured and revised manuscript; and AS, TA, and JO make comments on the manuscript.

Competing interest

The authors declare that they have no conflict of interest.

Acknowledgments

Authors thank anonymous reviewers for their professional review, understanding of our study topic, and constructive comments on the manuscript for significant improvement; Brittney Smart for her professional proofreading; Rex Burgon for his advices about the technical design of a CPEC sampling system; and Edward Swiatek for his setting the CPEC system in Campbell Scientific Instrument Test Field. This research was supported by the Strategic Priority Research Program of the Chinese Academy of Sciences (XDA19030204), Chinese Academy of Sciences President's International Fellowship Initiative (2020VBA0007), Long Term Agroecosystem Network (LTAR-USD), and Campbell Scientific Research and Development.

References

AmeriFlux: data variables, Lawrence Berkeley National Laboratory, http://ameriflux.lbl.gov/data/aboutdata/data-variables/, 1–12 pp., 2018.

Apogee Instrument, Inc: owner's manual: aspirated radiation shield (model: TS-100), Logan, UT, USA, 19 p., 2013.

Aubinet, M., Vesala, T., and Papale, D. (Ee~~.~~ds)~~.~~ Eddy Covariance: A Practice Guide to Measurement and Data Analysis. Springer, ~~New York~~, NY, USA, 438 p., 2012.

Barrett, E. W. and Suomi, V. E.: Preliminary report on temperature measurement by sonic means, J. Atmos. Sci., 6, 273–276, 1949.

Blonquist, J. M. and Bugbee, B.: Air temperature, in: agroclimatology: linking agriculture to climate, Agronomy Monographs, edited by: Hatfield, J., Sivakumar, M., and Prueger, J., American Society of Agronomy, Crop Science Society of America, and Soil Science Society of America, Inc., Madison, WI, USA, 2018.

Burden, R.L. and Faires, J.D: Numerical analysis (5th ed), PWS Publishing Company, Boston, MA, USA, 768 p., 1993.

Burgon, R. P., Jr., Sargent, S., Zha, T., and Jia, X.: Field performance verification of carbon dioxide, water, and nitrous oxide closed-path eddy covariance systems with vortex intakes, in: AGU Fall Meeting Abstracts, San Francisco, CA, USA, 14-18 December 2015, B33C-0669, 2015.

Campbell, G.S.: Measurement of air temperature fluctuations with thermocouples. Atmospheric Sciences Laboratory, White Sands Missile Range, ~~New Mexico~~, NM, USA~~.~~ ECOM-5273, 17 pp., 1969.

Campbell Scientific Inc: Model ASPTC aspirated shield with fine wire thermocouple. Revision 6/10, Logan, UT, USA, 8 p., 2010.

Campbell Scientific Inc: CPEC300/306/310 Closed-Path Eddy-Covariance Systems, Revision 10/18, Logan, UT, USA, 8 p., 2018a.

Campbell Scientific Inc: CSAT3B three-dimensional sonic anemometer, Revision 3/18, Logan, UT, USA, 58 p., 2018b.

Campbell Scientific Inc: EC155 CO_2/H_2O closed-path gas analyzer, Revision 7/18, Logan, UT, USA, 5–7 pp., 2018c.

Foken, T., Aubinet, M., and Leuning, R.: The eddy covariance method, in: eddy covariance: a practical guide to measurement and data analysis, edited by: Aubinet, M., Vesala, T., and Papale, D., Springer Netherlands, Dordrecht, 1–19 pp., 2012.

Gill Instruments: Horizontally symmetrical research ultrasonic anemometer: user manual, document number: 1199-PS-0003, Issue 08, Hampshire, UK, 70 p., 2004.

Gu, L., Massman, W. J., Leuning, R., Pallardy, S. G., Meyers, T., Hanson, P. J., Riggs, J. S., Hosman, K. P., and Yang, B.: The fundamental equation of eddy covariance and its application in flux measurements, Agr. Forest Meteorol., 152, 135–148, doi:10.1016/j.agrformet.2011.09.014, 2012.

Helbig, M., Wischnewski, K., Gosselin, G. H., Biraud, S. C., Bogoev, I., Chan, W. S., Euskirchen, E. S., Glenn, A. J., Marsh, P. M., Quinton, W. L., and Sonnentag, O.: Addressing a systematic bias in carbon dioxide flux measurements with the EC150 and the IRGASON open-path gas analyzers, Agr. Forest Meteorol., 228–229, 349–359, doi:10.1016/j.agrformet.2016.07.018, 2016.

Horst, T.W. and Lenschow, D.H.: Attenuation of scalar fluxes measured with spatially-displaced sensors, Boundary-Layer Meteorology, 130, 275-300, doi:10.1007/s10546-008-9348-0, 2009.

Ibrom, A., Dellwik, E., Flyvbjerg, H., Jensen, N. O., and Pilegaard, K.: Strong low-pass filtering effects on water vapour flux measurements with closed-path eddy correlation systems, Agr. Forest Meteorol., 147, 140–156, doi:10.1016/j.agrformet.2007.07.007, 2007.

International Organization for Standardization: Accuracy (trueness and precision) of measurement methods and results-Part 1: General principles and definitions. ISO 5725-1. 1994 (reviewed in 2012). 17p., 2012.

Irwin, H. P. A. H.: Cross-spectra of turbulence velocities in isotropic turbulence, Boundary-Layer Meteorology, 16, 237–243, doi:10.1007/BF03335368, 1979.

Ishii, C.: Supersonic velocity in gases: especially in dry and humid air. Scientific Papers of the Institute of Physical and Chemical Research, Tokyo, 26, 201–207 pp., 1932.

Kaimal, J. C. and Businger, J. A.: A continuous wave sonic anemometer-thermometer, Journal of Applied Meteorology, 2, 156–164, doi:10.1175/1520-0450(1963)0022.0.CO;2, 1963.

Kaimal, J. C. and Finnigan, J. J. (Eds.): Atmospheric boundary layer flows: their structure and measurement, Oxford University Press, Oxford, 289, 1994.

Kaimal, J. C. and Gaynor, J. E.: Another look at sonic thermometry, Boundary-Layer Meteorology, 56, 401–410, doi:10.1007/BF00119215, 1991.

Laubach, J. and McNaughton, K. G.: A spectrum-independent procedure for correcting eddy fluxes measured with separated sensors, Boundary-Layer Meteorology, 89, 445–467, doi:10.1023/A:1001759903058, 1998.

Lee, X., and Massman, W.J.: A perspective on thirty years of the Webb, Pearman and Leuning density corrections, Boundary-Layer Meteorology, 139, 37–59, doi:10.1007/s10546-010-9575-z, 2011.

LI-COR Biosciences: EddyPro® eddy covariance software: instruction manual, Lincoln, NE, USA, 1—1 to 10—6 pp., 2015.

LI-COR Biosciences: LI-7500RS open path CO_2/H_2O gas analyzer: instruction manual, Lincoln NE, 4-1–11 and 8-1–9 pp., 2016.

Lin, X., Hubbard, K. G., Walter-Shea, E. A., Brandle, J. R., and Meyer, G. E.: Some perspectives on recent in situ air temperature observations: modeling the microclimate inside the radiation shields, J. Atmos. Ocean. Tech., 18, 1470–1484, 2001.

Liu, H., Peters, G. and Foken, T.: New equations for sonic temperature variance and buoyancy heat flux with an omnidirectional sonic anemometer, Boundary-Layer Meteorology, 100, 459–468, doi:10.1023/A:1019207031397, 2001.

Ma, J., Zha, T., Jia, X., Sargent, S., Burgon, R., Bourque, C. P. A., Zhou, X., Liu, P., Bai, Y., and Wu, Y.: An eddy-covariance system with an innovative vortex intake for measuring carbon dioxide and water fluxes of ecosystems, Atmos. Meas. Tech., 10, 1259–1267, doi:10.5194/amt-10-1259-2017, 2017.

Mahan, H., Gao, T., Li, X., Forbush, T., Payne, K., Yang, Q., Li, Y., Zhou, H., Wu, S., Zheng, N., and Zhou, X.: Weather-condition-regulated, heated 3-D sonic anemometers (CSAT3AH and CSAT3BH): Working rationale, operation algorithm, and performance assessment, EGU General Assembly 2021, online, 19–30 Apr 2021, EGU21-13671, https://doi.org/10.5194/egusphere-egu21-13671, 2021.

Moncrieff, J. B., Massheder, J. M., de Bruin, H., Elbers, J., Friborg, T., Heusinkveld, B., Kabat, P., Scott, S., Soegaard, H., and Verhoef, A.: A system to measure surface fluxes of momentum, sensible heat, water vapour and carbon dioxide, J. Hydrol., 188–189, 589–611, doi:10.1016/S0022-1694(96)03194-0, 1997.

Moore, C. J.: Frequency response corrections for eddy correlation systems, Boundary-Layer Meteorology, 37, 17–35, doi:10.1007/BF00122754, 1986.

Munger, J. W., Loescher, H. W., and Luo, H.: Measurement, tower, and site design considerations, in: eddy covariance: a practical guide to measurement and data analysis, edited by: Aubinet, M., Vesala, T., and Papale, D., Springer Netherlands, Dordrecht, 21–58, 2012.

Panofsky, H.A. and Dutton, J.A. (Eds): Atmospheric Turbulence: Model and Methods for Engineering Applications. John Wiley & Sons, NY, USA, 397 p, 1984.

Rebmann, C., Kolle, O., Heinesch, B., Queck, R., Ibrom, A., and Aubinet, M.: Data acquisition and flux calculations, in: Eddy covariance: a practical guide to measurement and data analysis, edited by: Aubinet, M., Vesala, T., and Papale, D., Springer Netherlands, Dordrecht, 59–83, 2012.

R.M. Young Company. Compact aspirated radiation shield: Model 43502, Traverse City, MI, USA, 1–4 pp., 2004.

Saramäki, T.: Finite impulse response filter design, in: Handbook for digital signal processing, edited by: Mitra, K.S. and Kaiser, J.F., John Wiley & Sons, Inc., New York, NY, 155–277, 1993.

Schotanus, P., Nieuwstadt, F. T. M., and De Bruin, H. A. R.: Temperature measurement with a sonic anemometer and its application to heat and moisture fluxes, Boundary-Layer Meteorology, 26, 81-93, doi:10.1007/BF00164332, 1983.

Snedecor, G.W and Cochran, W.G. (Eds.): Statistical Methods (8^{th} ed), Iowa State University Press, Ames, IA, USA, 502, 1989.

Sonntag, D.: Important new values of the physical constants of 1986, vapour pressure formulations based on the ITS-90, and psychrometer formulae, Z. Meteorol., 40, 340–344, 1990.

Stull, R.B. (Eds.): An introduction to boundary layer meteorology, Kluwer Academic Publisher, Dordrecht, 35–437, 1988.

Swiatek, E.: Derivation of the calculated sensible heat flux (H_c) from the sonic sensible heat flux (H_s) and latent heat flux (LE). Campbell Scientific Inc, Logan, UT, 1–2 pp., 2009.

Swiatek, E: Derivation of Temperature (T_c) from the Sonic Virtual Temperature (T_s), vapor density (ρ_v)/vapor pressure (e) and pressure (P). Campbell Scientific Inc. Logan, UT, 1-5 pp., 2018.

van Dijk, A.: The principles of surface flux physics. Department of Meteorology and Air Quality, Agriculture University

Wageningen, 40–41 pp., 2002.

Wallace, J. M. and Hobbs, P. V. (Eds.): Atmospheric science: an introductory survey, Academic Press, London, 350, 2006.

Wang, W., Xu, J., Gao, Y., Bogoev, I., and Lee, X.: Performance evaluation of an integrated open-path eddy covariance system in a cold desert environment, J. Atmos. Ocean. Tech., 33, 274–283, 2016.

Webb, E.K., Pearman, G.I., and Leuning, R.: Correction of flux measurements for density effects due to heat and water vapour transfer, Quarterly Journal of the Royal Meteorological Society, 106, 85-100, doi:10.1002/qj.49710644707, 1980.

Wright, J. D., Johnson, A. N., and Moldover, M. R.: Design and Uncertainty for a PVTt Gas Flow Standard. Journal of Research of the National Institute of Standards and Technology, 108 (1), 21–47, doi:10.6028/jres.108.00, 2003.

Zhou, X., Gao, T., Pang, Y., Manhan, H., Li, X., Zheng, N., Suyker, A.E., Awada, T., Zhu., J.: Based on atmospheric physics and ecological principle to assess the accuracies of field CO_2/H_2O measurements from infrared gas analyzers in closed-path eddy-covariance systems. Earth and Space Science, inpress, doi:10.1029/2021EA001763, 2021.

Zhou, X., Yang, Q., Zhen, X., Li, Y., Hao, G., Shen, H., Gao, T., Sun, Y., and Zheng, N.: Recovery of the three-dimensional wind and sonic temperature data from a physically deformed sonic anemometer, Atmos. Meas. Tech., 11, 5981–6002, doi:10.5194/amt-11-5981-2018, 2018.

Zhu, J., Gao, T., Yu, L., Yu, F., Yang, K., Lu, D., Yan, Q., Sun, Y., Liu, L., Xu, S., Zhang, J., Zheng, X., Song, L., and Zhou, X. Functions and applications of Multi-Tower Platform of Qingyuan Forest Ecosystem Research Station of Chinese Academy of Sciences (Qingyuan Ker Towers). Bulletin of Chinese Academy of Sciences 3, 351-361, doi:10.16418/jissn.1000-3045.20210304002, 2021.